Journal of Biological Chemistry. (2008) 283(43): 29144-29155.

Roles of Tyrˆ<122>-hydrophobic Cluster and Kˆ+ Binding in Caˆ<2+>-releasing Process of ADP-insensitive Phosphoenzyme of Sarcoplasmic Reticulum Caˆ<2+>-ATPase.

Yamasaki K, Wang G, Daiho T, Danko S, Suzuki H.

Roles of Tyr^{122}-Hydrophobic Cluster and K^+ Binding in Ca^{2+}-releasing Process of ADP-insensitive Phosphoenzyme of Sarcoplasmic Reticulum Ca^{2+}-ATPase*

Kazuo Yamasaki, Guoli Wang, Takashi Daiho, Stefania Danko, and Hiroshi Suzuki

Department of Biochemistry, Asahikawa Medical College, Asahikawa 078-8510, Japan

Running Title: Tyr^{122}-Hydrophobic Cluster of SERCA1a for Ca^{2+} Release

Correspondence address to: Kazuo Yamasaki, Dept. of Biochemistry, Asahikawa Medical College, Midorigaoka-Higashi, Asahikawa, 078-8510, Japan, Tel.: +81-166-68-2353; Fax: +81-166-68-2359; E-mail: kyamasak@asahikawa-med.ac.jp.

Tyr^{122}-Hydrophobic cluster (Y122-HC) is an interaction network formed by the top part of second transmembrane helix and the cytoplasmic Actuator and Phosphorylation domains of sarcoplasmic reticulum Ca^{2+}-ATPase. We have previously found that Y122-HC plays critical roles in the processing of ADP-insensitive phosphoenzyme (*E*2P) after its formation by the isomerization from ADP-sensitive phosphoenzyme (*E*1PCa_2) (Wang *et al.* (2005) *J. Biol. Chem.* 280, 26508-26516). Here, we further explored kinetic properties of the alanine-substitution mutants of Y122-HC to examine roles of Y122-HC for Ca^{2+}-release process in *E*2P. In the steady state, the amount of *E*2P decreased thereby that of *E*1PCa_2 increased with increasing lumenal Ca^{2+} concentration in the mutants with $K_{0.5}$ 110 ~ 320 μM at pH 7.3. These lumenal Ca^{2+} affinities in *E*2P agreed with those estimated from the forward and lumenal Ca^{2+}-induced reverse kinetics of the *E*1PCa_2-*E*2P isomerization. $K_{0.5}$ of the wild type was estimated to be 1.5 mM in this kinetics. Thus, *E*2P of the mutants possess significantly higher affinities for lumenal Ca^{2+} than that of the wild type. The kinetics further indicated that the rates of lumenal Ca^{2+} access and binding to the transport sites of *E*2P were substantially slowed by the mutations. Therefore the proper formation of Y122-HC and resulting compactly organized structure is critical for both decreasing Ca^{2+} affinity and opening the lumenal gate, thus for Ca^{2+} release from *E*2PCa_2. Interestingly, when K^+ was omitted from the medium of the wild type, the properties of the wild type became similar to those of Y122-HC mutants. K^+ binding likely functions *via* producing the compactly organized structure, in this sense, similarly to Y122-HC.

Sarcoplasmic reticulum Ca^{2+}-ATPase (SERCA1a[1]) of the P-type ion transporting ATPase family catalyzes Ca^{2+} transport coupled with ATP hydrolysis from the cytoplasm to lumen against ~10000-fold concentration gradient (Refs. 1-8). In the initial steps (steps 1 and 2 in Scheme 1), the enzyme is activated by binding of two cytoplasmic Ca^{2+} ions at the transport sites with a submicromolar high affinity (*E*2 to *E*1Ca_2). The activated enzyme is then auto-phosphorylated at Asp^{351} by ATP and forms a phosphoenzyme intermediate (*E*P) (step 3), thereby the bound Ca^{2+} ions are occluded in the transport sites. This *E*P is rapidly dephosphorylated by ADP in the reverse reaction reproducing ATP, therefore "ADP-sensitive *E*P" (*E*1P). In the next step (step 4), *E*1PCa_2 is isomerized to the ADP-insensitive form, *E*2PCa_2. Upon this change at the catalytic site, the Ca^{2+} sites are deoccluded and opened to the lumenal side and the Ca^{2+} affinity is largely reduced, releasing the bound Ca^{2+} ions into the lumen (step 5). The Ca^{2+}-release process is thought to be very rapid with the wild type Ca^{2+}-ATPase, and the accumulation of *E*2PCa_2 intermediate had actually never been found until we recently identified and trapped successfully this intermediate by a mutation study (9). In the final step, the Asp^{351}-acylphosphate of *E*2P is hydrolyzed to reproduce the dephosphorylated and inactive *E*2 form (step 6). The transport cycle is totally reversible, *e.g.* *E*2P can be formed from *E*2 by P_i in the absence of Ca^{2+}, and the subsequent lumenal Ca^{2+} binding to *E*2P produces *E*1PCa_2.

Three-dimensional structures in several intermediate states and their analogs have been solved (10-18). The Ca^{2+}-ATPase has three cytoplasmic domains; P (phosphorylation), N (nucleotide binding), and A (actuator or

anchor), and ten transmembrane helices (M1-M10). The two Ca^{2+} binding sites consist of residues on the M4, M5, M6, and M8 (10). The P domain possesses the phosphorylation site (Asp^{351}) and is directly linked to the long helices M4 and M5. The ATP binding site is on the N domain connected to the P domain. The A domain is linked to M1, M2, and M3 *via* the A/M1-, A/M2- and A/M3-linkers. The cytoplasmic three domains largely move and change their organization states during the Ca^{2+}-transport cycle (19-21), and these changes are linked with the rearrangements in the transmembrane helices for the Ca^{2+} transport. As a most remarkable change, in the *E*P isomerization (loss of ADP-sensitivity) and Ca^{2+} release, the A domain largely rotates and the P domain largely inclines toward the A domain and these domains produce their tight association (see Fig. 1 for the change $E1Ca_2 \cdot AlF_4^- \cdot ADP \rightarrow E2 \cdot MgF_4^{2-}$ as the model for the overall process $E1 \sim PCa_2 \cdot ADP \rightarrow E2 \cdot P_i$ including the *E*P isomerization and Ca^{2+} release). These structural changes therefore involve distinct events in distinct regions, yet they are coordinated; namely 1) the loss of ADP-sensitivity at the cytoplasmic region, 2) the decrease in the Ca^{2+}-affinity at the transmembrane region, 3) the opening of the Ca^{2+}-releasing pathway (lumenal gating).

Recently, we found that mutations in a specific hydrophobic interaction network, "Tyr^{122}-hydrophobic cluster" (Y122-HC) at the A-P domain interface disrupt markedly the processing of ADP-insensitive *E*P formed from ATP with Ca^{2+} and also the hydrolysis of *E*2P formed from P_i without Ca^{2+}, thus causing nearly complete inhibition of the Ca^{2+}-ATPase activity (22, 23). In these Y122-HC mutants, the high affinity binding of cytoplasmic Ca^{2+}, the resulting $E1PCa_2$ formation, and the loss of the ADP-sensitivity were all found to occur normally as in the wild type (22, 23). Y122-HC is formed by gathering of the seven residues of the three regions upon their motions; *i.e.* the largely rotated A domain (Ile^{179}, Leu^{180}, and Ile^{232}), the inclined P domain (Val^{705} and Val^{726}), and the top part of the largely inclined M2 (or the A/M2-linker) (Leu^{119} and Tyr^{122}). Thus Y122-HC produces the compactly organized structure of *E*2P. Our previous analyses indicated that in the Y122-HC mutants, there is a kinetic limit after the loss of ADP-sensitivity and before the hydrolysis of the Ca^{2+}-free *E*2P, therefore the Ca^{2+} release from $E2PCa_2$ is likely retarded (22, 23). Almost the same kinetic results were found with the mutations in another A-P domain interaction network at the Val^{200} loop of the A domain (24). Notably, $E2PCa_2$, the ADP-insensitive *E*P with two Ca^{2+} ions occluded at the transport sites was recently identified and trapped successfully by the elongation of the A/M1-linker with two or more amino-acid insertions (9). In the elongation mutants, Y122-HC is not formed properly yet in $E2PCa_2$ trapped, but it is properly formed in the Ca^{2+}-released form of *E*2P produced by P_i without Ca^{2+}. Thus the observation is consistent with the involvement of Y122-HC in the Ca^{2+}-release process from $E2PCa_2$.

In this study, to further clarify roles of Y122-HC in the Ca^{2+}-deocclusion/release processes and thus in the long-range communication between the cytoplasmic and transmembrane regions, we explored kinetic features of the alanine-substitution mutants of Y122-HC. The results revealed that the mutations cause a marked increase in the apparent affinity of *E*2P for lumenal Ca^{2+} and also a substantial retardation of the lumenal Ca^{2+} access to *E*2P. Therefore, the formation of Y122-HC is critical for decreasing the affinity for Ca^{2+}, for lumenal gating (opening of the release pathway), and thus for Ca^{2+} release into lumen. Importantly, the assembling manner of the seven residues in Y122-HC in the very recently revealed crystal structure $E2 \cdot BeF_3^-$ (17, 18) somewhat differs from that in $E2 \cdot AlF_4^-$ and $E2 \cdot MgF_4^{2-}$. Therefore we discussed the significance of this difference in terms of the possible sequential gathering of the seven residues into Y122-HC on the basis of the observed difference in the extents of the mutational effects of the seven residues in Y122-HC. In addition, we found with the wild type that its kinetic behavior became similar to that of Y122-HC mutants when K^+ was omitted from the medium of the wild type. Results revealed for the first time the critical role of K^+ binding in the wild type for Ca^{2+}-deocclusion/release from $E2PCa_2$.

EXPERIMENTAL PROCEDURES

Mutagenesis and Expression — Mutations were created by the QuikChange™ site-directed mutagenesis kit (Stratagene) and plasmid pGEM7-Zf(+) or pGEM3-Zf(+) (Promega) containing ApaI-KpnI or KpnI-SalI fragments of rabbit SERCA1a cDNA as a template. The ApaI-KpnI or KpnI-SalI fragments were then excised from the products and used to replace the corresponding region in the full-length SERCA1a cDNA in the pMT2

expression vector (25). The pMT2 DNA was transfected into COS-1 cells by the liposome-mediated transfection method. Microsomes were prepared from the cells as described previously (26). The "control microsomes" were prepared from COS-1 cells transfected with the pMT2 vector containing no SERCA1a cDNA.

ATPase Activity — The rate of ATP hydrolysis was determined at 25 °C in a mixture containing 20 μg/ml microsomal protein, 0.1 mM [γ-^{32}P]ATP, 3 μM A23187, 0.1 M KCl, 7 mM $MgCl_2$, various concentrations of $CaCl_2$ up to 3 mM, 0.01 mM EGTA, and 50 mM MOPS/Tris (pH 7.3).

Formation and Hydrolysis of EP — Phosphorylation of SERCA1a in microsomes with [γ-^{32}P]ATP or $^{32}P_i$, and dephosphorylation of ^{32}P-labeled SERCA1a was performed under conditions described in the figure legends. The reactions were quenched with ice-cold trichloroacetic acid containing P_i. Rapid kinetics measurements of phosphorylation and dephosphorylation were performed with a handmade rapid mixing apparatus (27), otherwise the method was as above. The precipitated proteins were separated at pH 6.0 by 5% SDS-polyacrylamide gel electrophoresis, according to Weber and Osborn (28). The radioactivity associated with the separated Ca^{2+}-ATPase was quantitated by digital autoradiography as described previously (29). The amount of *E*P formed with the expressed SERCA1a was obtained by subtracting the background radioactivity with the control microsomes. This background was less than 1% of the radioactivity of *E*P formed with the expressed wild-type SERCA1a.

Miscellaneous — Protein concentrations were determined by the method of Lowry *et al*. (30) with bovine serum albumin as the standard. Free Ca^{2+} concentrations were calculated by the Calcon program. Data were analyzed by nonlinear regression using the program Origin (Microcal Software, Inc., Northampton, MA). Three-dimensional models of the enzyme were reproduced by the program VMD (31).

RESULTS

Ca^{2+}-induced Change in Accumulation of ADP-insensitive EP in the Presence of 0.1 M K^+ at Steady State — We first determined the steady state Ca^{2+}-ATPase activity in the presence of increasing Ca^{2+} and ionophore A23187 with the alanine-substitution mutants of the seven residues of Y122-HC and the wild type. The Ca^{2+}-ATPase activity was nearly completely inhibited in all the mutants in agreement with our previous observation (22, 23), and the complete inhibition was found at all the Ca^{2+} concentrations examined (see Supplemental Figure 1 for the representative mutant Y122A). Thus the possible lumenal Ca^{2+} effect was not revealed by this type of measurements. Therefore in Fig. 2, to assess the affinity of the lumenally oriented Ca^{2+} transport site of *E*2P (known as the low affinity sites with the mM ~ over 10 mM K_d value), the amounts of ADP-insensitive *E*P were determined with the representative mutant Y122A at steady state at various Ca^{2+} concentrations and pHs in the presence of A23187 and KCl. The total amounts of *E*P (ADP-sensitive *E*P plus ADP-insensitive *E*P) were nearly the same under all the sets of conditions.

In the mutant Y122A, the fraction of the ADP-insensitive *E*P was very high at the low Ca^{2+} concentrations at all pHs (Fig. 2). This agrees with the property of this mutant (22, 23) that the hydrolysis of *E*2P is nearly completely inhibited thus causing its accumulation. The fraction of ADP-insensitive *E*P in the mutant markedly decreased and it was converted to the ADP-sensitive *E*P with increasing Ca^{2+} concentration at several tens μM to sub-mM range. The apparent Ca^{2+} affinity in this Ca^{2+}-induced change increased with increasing pH and the Hill coefficients were found to be 2 in all pHs (see the legend to Fig. 2). In the wild type, the fraction of ADP-insensitive *E*P was low at pH 7.3 and 7.8 being approximately 10% or less, and was a significant level, 35% at pH 6.8 (Supplemental Figure 2). These levels were not changed at 1 μM to 3 mM Ca^{2+}. Consistently, the lumenal Ca^{2+} affinity of *E*2P of the wild type is known to be mM ~ 10 mM range (*see* Ref. 32-34). The results suggested that the lumenal Ca^{2+} affinity of transport sites of *E*2P in the mutant may be significantly higher than that in the wild type.

Time Courses of Forward and Ca^{2+}-induced Reverse Conversions between $E1PCa_2$ and E2P — In Fig. 3 with Y122A, the ADP-insensitive *E*P and the ADP-sensitive *E*P was first accumulated at steady state at 10 μM Ca^{2+} and 1 mM Ca^{2+}, respectively at pH 7.3. Then the Ca^{2+} concentration jump was made from 10 μM to 1 mM or from 1 mM to 80 nM, and the change in the fraction of the ADP-insensitive *E*P was followed. Because the hydrolysis of *E*2P was nearly completely blocked in Y122A

(with the rate << $0.01 s^{-1}$) (22, 23), the time courses represent the forward and reverse isomerization between $E1PCa_2$ and $E2P$. When Ca^{2+} was increased from 10 μM to 1 mM, the fraction of ADP-insensitive EP rapidly decreased from 80% to 10% (*i.e.* it was converted to the ADP-sensitive EP) with a rate 0.4 s^{-1}. On the other hand, when the Ca^{2+} concentration was decreased from 1 mM to 80 nM, *i.e.* virtually Ca^{2+} was removed, the ADP-sensitive EP was converted to the ADP-insensitive EP with a rate 0.022 s^{-1}.

Effect of Ca^{2+} Ionophore A23187 in Accumulation of ADP-insensitive EP — To ascertain that the Ca^{2+} dependent changes in the fraction of ADP-insensitive EP (Figs. 2 and 3) are caused by lumenal Ca^{2+}, we examined also in the absence of A23187 the Ca^{2+} dependence of the steady state fraction of ADP-insensitive EP (Fig. 4). The Ca^{2+} dependent change was rather small in the absence of A23187, in contrast to the very large change in its presence. Therefore, the observed Ca^{2+}-induced conversion from the ADP-insensitive EP to ADP-sensitive one in Y122A is due to the Ca^{2+} binding to the lumenally oriented transport sites.

Ca^{2+}-induced Change in Accumulation of ADP-insensitive EP of Seven Y122-HC Mutants in the Presence of 0.1 M K^+ — In Fig. 5, each of the other six residues involved in the Y122-HC (Leu^{119}/Ile^{179}/Leu^{180}/Ile^{232}/Val^{705}/Val^{726}) was substituted with alanine, and its effect on the ADP-insensitive EP level was examined as in Fig. 2 in the presence of A23187 and K^+. All the Y122-HC mutants exhibited the marked Ca^{2+}-dependent change in the ADP-insensitive EP fraction[2]. The apparent affinities for lumenal Ca^{2+} in the Y122-HC mutants were found to be between 110 and 320 μM with the Hill coefficients approximately 2 (Table 1). The results showed that all these Y122-HC mutants possess the lumenally oriented transport sites with the affinities as high as that of Y122A.

Ca^{2+}-induced Change in Accumulation of ADP-insensitive EP of Mutants and Wild Type in the Absence of K^+ — In Fig. 6, the same sets of steady-state analysis as in Fig. 2 were done with the wild type and Y122A but here in the absence of K^+. It is well known (35, 36) that in the absence of K^+, the $E2P$ hydrolysis of the wild type is markedly slowed and therefore the ADP-insensitive EP significantly accumulates. The fraction of ADP-insensitive EP in the wild type in the absence of K^+ decreased with increasing Ca^{2+} concentration as in Y122A with the Hill coefficient approximately 2. The apparent affinity for lumenal Ca^{2+} increased with increasing pH in the wild type as in Y122A. The pH dependent changes are consistent with the fact that the residues for Ca^{2+} ligation at the transport sites are also involved in the proton binding (and its counter transport); the observed Ca^{2+}-induced changes reflect the Ca^{2+} binding to the lumenally oriented transport sites of $E2P$. At each pH, the affinity of the wild type was similar to or slightly lower than that of Y122A. Thus in the absence of 0.1 M K^+, the property of the wild type became similar to that of Y122A. In Y122A, elimination of K^+ exhibited no significant effect on the apparent affinity for lumenal Ca^{2+} (*cf.* Fig. 2).

The observed effect of K^+ on the wild type is probably due to its binding at cytoplasmic region. In the crystallographic as well as mutational studies (12, 37), the K^+ binding site of the Ca^{2+}-ATPase was identified to be in the cytoplasmic region but not in the lumenal or transmembrane regions (see Fig. 11). Actually, we found experimentally that when K^+ at 0.1 M was added without any K^+-ionophore to the Ca^{2+}-ATPase in SR vesicles phosphorylated in the absence of K^+, the Ca^{2+}-dependence of the ADP-insensitive EP fraction observed as in Fig. 6*A* became immediately (within 10 sec after the K^+ addition) that in the presence of 0.1 M K^+ as in Supplemental Figure 2 (data not shown).

Kinetics of Lumenal Ca^{2+}-induced E2P to $E1PCa_2$ Reverse Transition Followed by Its ADP-induced Rapid Decay to $E1Ca_2$ in the Presence of 0.1 M K^+ — Then with the representative mutant Y122A, we explored kinetically the lumenal Ca^{2+} accessibility to the lumenally oriented transport sites of $E2P$ formed from P_i without Ca^{2+} and the resulting lumenal Ca^{2+}-induced $E2P$ to $E1PCa_2$ reverse transition. In Fig. 7, we included ADP and thereby followed the Ca^{2+}- and ADP-induced decay of $E2P$ to $E1Ca_2$ *via* $E1PCa_2$ in the reverse reaction. The $E2P$ hydrolysis in the absence of Ca^{2+} was extremely slow (as previously demonstrated with the Y122-HC mutants (22, 23)), and the $E2P$ decay was dramatically accelerated by the addition of Ca^{2+} and ADP (Fig. 7*A*). For example, the rate in the presence of 1 mM Ca^{2+} was 200-times faster than that of the forward $E2P$ hydrolysis in the absence of Ca^{2+}. ADP alone without Ca^{2+} or Ca^{2+} alone without ADP did not accelerate the EP decay (data not shown). As shown in Fig. 3, the increase of Ca^{2+} to 1 mM converted the ADP-insensitive EP ($E2P$) to the ADP-sensitive one ($E1PCa_2$), and $E1PCa_2$ thus

formed was not decomposed in the absence of ADP. Therefore the Ca^{2+}- and ADP-induced decay of *E*2P in Fig. 7*A* obviously occurred in the reverse reaction by the lumenal Ca^{2+} binding; *E*2P + $2Ca^{2+}$ → *E*1PCa_2, then *E*1PCa_2 + ADP → *E*1Ca_2 + ATP (Scheme 1). This view agrees with the previous demonstration with SR Ca^{2+}-ATPase (34). The rate of the *E*P decay in the presence of Ca^{2+} and ADP increased almost linearly with increasing Ca^{2+} concentrations and was not saturated even at 3 mM (Fig. 7*B*)[3]. Here, note that the steady state level of ADP-sensitive *E*P (*E*1PCa_2) in the conversion from the ADP-insensitive *E*P (*E*2P) upon the lumenal Ca^{2+} binding in Y122A was almost fully saturated at 1 mM Ca^{2+} (see Fig. 2 at pH 7.3). The results indicate that the lumenal Ca^{2+} binding to *E*2P and formation of *E*2PCa_2 (*E*2P + $2Ca^{2+}$ → *E*2PCa_2) is likely the rate-limiting for the overall Ca^{2+}- and ADP-induced reverse decay *via* the *E*2P to *E*1PCa_2 conversion with subsequent extremely rapid ADP-induced *E*1PCa_2 decay to *E*1Ca_2. This means that the slope in Fig. 7*B* in the Ca^{2+} dependence probably reflects the rate constant for the lumenal Ca^{2+} access and binding to the lumenally oriented transport sites of *E*2P and resulting *E*2PCa_2 formation.

The Ca^{2+}- and ADP-dependent acceleration of the reverse *E*2P decay was assayed also with all the other Y122-HC mutants (Supplemental Figure 3). The rates of the reverse *E*2P decay increased almost linearly with increasing Ca^{2+} concentrations even at 3 mM, except those of I232A and V705A[4] over ~1 mM Ca^{2+}. Nevertheless, the slope of the Ca^{2+} dependence below 1 mM Ca^{2+} was estimated to be approximately 0.2 $s^{-1}mM^{-1}$ in all the mutants as in Y122A. Therefore, the rate of the lumenal Ca^{2+} access and binding to the transport sites is similar in all the mutants of Y122-HC.

Kinetics of Lumenal Ca^{2+} Access to E2P of Wild Type and Y122A with and without K^+ — Then in Fig. 8, with the wild type and the representative mutant Y122A in the presence and absence of 0.1 M K^+, we analyzed the Ca^{2+}- and ADP-dependent acceleration of the reverse decay of *E*2P formed from P_i without Ca^{2+}. As the well characterized property of the wild type, the forward hydrolysis of *E*2P without bound Ca^{2+} is very slow in the absence of K^+, but markedly accelerated and thus very rapid in the presence of 0.1 M K^+ (35, 36) (see the rates without Ca^{2+} in Fig. 8*A*). Nevertheless, even with the wild type in the presence of K^+, we observed an apparently single exponential decay of *E*2P after the addition of Ca^{2+} and ADP at all the Ca^{2+} concentrations examined (time courses are not shown for simplicity). This is consistent with the kinetics described in the textbook by Fersht (39) that in the parallel reactions in which a compound undergoes two or more single-step reactions simultaneously, its disappearance rate is described by a single exponential decay. In our case, the two reactions are the forward *E*2P hydrolysis and the Ca^{2+}-/ADP-induced reverse *E*2P decay. The single decay rates thus obtained are plotted in Fig. 8*A*.

In the wild type in the presence of 0.1 M K^+, the Ca^{2+} dependence of the *E*P decay rate was complicated because of the rapid *E*2P hydrolysis without Ca^{2+} (~0.4 s^{-1}), no change in the rate at 0~0.6 mM Ca^{2+}, and the gradual increase above 0.6 mM. On the other hand, in the wild type in the absence of K^+ in which the *E*2P hydrolysis without bound Ca^{2+} is markedly slowed, the nearly linear increase in the rate of Ca^{2+}-/ADP-induced reverse *E*2P decay was observed at least up to ~3 mM Ca^{2+} as in the Y122-HC mutants in the presence of K^+. The slope of the wild type without K^+ was actually close to that of Y122A with K^+. Therefore, the rate of lumenal Ca^{2+} access and binding to the transport sites of *E*2P of the wild type in the absence of K^+ is similar to that of Y122A. With the wild type in the presence of K^+, evaluation of the lumenal Ca^{2+} access rate by this approach was not possible because of the complicated Ca^{2+}-dependence curve. In Y122A, little effect was seen when K^+ was omitted at 0~1 mM Ca^{2+}, although the slope became gradually less steep at the higher Ca^{2+} concentration in the absence of K^+.

In Fig. 8*B*, by using the rates of the *E*2P decay in the presence of added Ca^{2+} and ADP (determined in Fig. 8*A*) and the rates of the forward *E*1PCa_2 to *E*2P transition (as determined in Fig. 3), we simulated the fraction of the steady-state level of the ADP-insensitive *E*P (*E*2P) in the total amount of *E*P at each Ca^{2+} concentration. Note that this simulation was made possible by the fact that nearly all the phosphorylation sites are phosphorylated at steady state (in either *E*1P or *E*2P form) under the conditions used for the steady-state and kinetic analyses at all the Ca^{2+} concentrations in this study. Namely, the *E*2 to *E*1Ca_2 transition and the *E*1PCa_2 formation from *E*1Ca_2 with ATP are rapid enough to be ignored from the simulation. Therefore, the fraction of ADP-insensitive *E*P (*E*2P) in the steady state will be determined by the rate of its formation in the forward *E*1PCa_2 to *E*2P transition, v_1, and by the rate of its decay, v_2

that includes both the forward hydrolysis of Ca^{2+}-unbound *E*2P to *E*2 and the Ca^{2+}-induced reverse transition to *E*1PCa_2 with the subsequent ADP-induced decay. This means that the simulation can be made even with the wild type in the presence of K^+ (as v_2 can include the forward *E*2P hydrolysis). In the steady-state conditions, the decay rate (v_2) and formation rate (v_1) should be equal, therefore the fraction of ADP-insensitive *E*P (F_{E2P}) in the total amount of *E*P will be estimated by an equation: $F_{E2P} = v_1/(v_1 + v_2)$. Here, the *E*2P decay rate (v_2) was obtained in Fig. 8*A* at each Ca^{2+} concentration. The *E*1PCa_2 to *E*2P transition rate (v_1) was estimated from the Ca^{2+} jump experiments from high (1 mM) to low (80 nM) for Y122A with and without 0.1 M K^+ and the wild type without K^+, as described in Fig. 3. With the wild type in the presence of 0.1 M K^+, the forward decay rate of *E*1PCa_2 formed by ATP was used as v_1, because the *E*1PCa_2 to *E*2P transition (the loss of ADP-sensitivity) is rate-limiting for the *E*1PCa_2 decay *via* *E*2P and its hydrolysis.

The Ca^{2+}-dependent curves thus obtained by the simulation for the steady-state level of ADP-insensitive *E*P for Y122A with and without K^+ and the wild type without K^+ agreed very well with the respective ones determined at the steady state (*cf.* Figs. 2 (with K^+) and 6 (without K^+) at pH 7.3). The affinities for lumenal Ca^{2+} estimated from the simulated curves are in fact almost the same as those actually determined at steady state (Table 2). The agreements assure the validity of the simulation and further allow us to estimate the lumenal Ca^{2+} affinity of *E*2P of the wild type in the presence of K^+. In the simulation for the wild type in the presence of K^+ (*open circles* and *inset* in Fig. 8*B*), the fraction of ADP-insensitive *E*P was very low and the extent of its change was extremely small as expected from the steady-state measurements (*cf.* Supplemental Figure 2 (pH 7.3)). The apparent affinity of wild type for lumenal Ca^{2+} in the presence of K^+ was thus estimated by the small change to be 1.5 mM (see Table 2). This affinity was approximately 3.5-times lower than that of wild type without K^+ and 10-times lower than that of Y122A with and without K^+. Thus by omitting K^+, the lumenal Ca^{2+} affinity of *E*2P in the wild type became higher and similar to that in Y122A.

Kinetics of Lumenal Ca^{2+}-induced E2P to E1PCa_2 Reverse Transition of E2P of Wild Type in the Presence of 0.1 M K^+ Was Revealed by the Absence of ADP — Unfortunately in the above experimental design and approach of Fig. 8*A*, we were not able to estimate the lumenal Ca^{2+} access rate in *E*2P of the wild type in the presence of K^+ because of the observed complexity of the Ca^{2+}-dependent curve. In Fig. 9, we therefore employed a modified and thus different approach to examine the lumenal Ca^{2+}-induced reverse conversion from *E*2P to *E*1PCa_2. Namely, *E*2P was formed with P_i and then a medium containing various concentrations of Ca^{2+} but without ADP (in contrast to its presence in Fig. 8) was added to *E*2P, and the subsequent *E*P decay was followed (Fig. 9*A*). In the absence of Ca^{2+}, *E*2P was all hydrolyzed rapidly to *E*2 in a single exponential function. The *E*2P hydrolysis was inhibited gradually with increasing Ca^{2+} concentrations (over 0.1 mM) and the decay time course became biphasic as typically seen with 1 mM Ca^{2+}. With increasing the Ca^{2+} concentration, the fraction of the first and rapid phase decreased, that of the second phase increased, and the rate of the second phase became further slower. The observation agrees with the previous kinetic analysis (9, 40). The first phase corresponds to the rapid and forward hydrolysis of the Ca^{2+}-unbound *E*2P to *E*2. The *E*P species in the second phase was all ADP-sensitive (data not shown), therefore *E*1PCa_2 formed from *E*2P by the lumenal Ca^{2+} binding. *E*1PCa_2 decayed very slowly in the absence of ADP because the *E*1PCa_2 to *E*2P transition is much slower than the *E*2P hydrolysis and this transition is retarded by the Ca^{2+} replacement of Mg^{2+} at the catalytic site of *E*1PCa_2 at the ~mM high Ca^{2+} concentrations (41, 42).

The fraction of the second and slow phase of the *E*P decay was obtained by extrapolating to the zero time, and plotted *versus* the Ca^{2+} concentration (Fig. 9*B*). The plot showed saturation at 5~10 mM Ca^{2+}. Here it is critical to note that, as previously discussed in detail (9), the fraction of *E*P of the second phase (the fraction remaining after the first phase) is dependent on the ratio between the rates of the forward *E*2P hydrolysis and of the reverse *E*2P to *E*1PCa_2 conversion upon the lumenal Ca^{2+} binding to *E*2P. Namely, the plot in Fig. 9*B* reflects the relation between these forward and reverse rates of *E*2P rather than the lumenal Ca^{2+} affinity of *E*2P. For example, at the 50% saturation of the curve, the rate of the Ca^{2+}-induced *E*1PCa_2 formation from *E*2P is equal to that of the *E*2P hydrolysis to *E*2. Then in Fig. 9*C* for the wild type in the presence of K^+, the rate of the *E*1PCa_2 formation from *E*2P by the lumenal Ca^{2+} binding to *E*2P was calculated (k_{rev}, *open circles*) at each Ca^{2+} concentration

by using the fraction of the slow and second phase (F_s) and the *E*2P hydrolysis rate (k_h) with the equation; $k_{rev} = k_h F_s/(1 - F_s)$. The rate increased largely with increasing Ca^{2+} concentration.

In this kinetics, we eliminated the contribution of forward *E*2P hydrolysis on the overall *E*2P decay kinetics, and thereby revealed the rate of reverse *E*2P transition to *E*1PCa_2 induced by the lumenal Ca^{2+} binding of the wild type in the presence of K^+. For comparison in Fig. 9*C*, the rates of the lumenal Ca^{2+}-induced reverse *E*2P decay estimated for the wild type without K^+ and Y122A with K^+ in Fig. 8*A* were replotted. Note again that in these cases, the hydrolysis of Ca^{2+}-unbound *E*2P was very slow and retarded; therefore the observed Ca^{2+}-/ADP-induced decay rates in their linear regions up to 3 mM Ca^{2+} reflect mostly the rates of the lumenal Ca^{2+} access and binding to *E*2P in the reverse *E*2P decay. Note also that the experimental design in Fig. 9*A* employed for the wild type with K^+ was not applicable to the wild type without K^+ and Y122A, because the *E*2P hydrolysis is very slow and almost completely retarded in these cases and therefore the *E*2P decay upon the Ca^{2+} addition can not be described as the biphasic decay. Conversely, the experimental design employed in Fig. 8*A* to estimate the rates of the lumenal Ca^{2+} access was not applicable to the wild type in the presence of K^+ because of the complexity of the Ca^{2+}-dependent curve as described above in Fig. 8*A*.

Thus in Fig. 9*C*, employing the inevitably different but most suitable experimental designs depending on the different kinetic properties, we were able to compare the rates of the *E*2P to *E*1PCa_2 reverse transition induced by the lumenal Ca^{2+} binding to the transport sites of *E*2P at the limited Ca^{2+} concentration range up to 3 mM. In the wild type in the presence of K^+, the rate was Ca^{2+} dependent and not saturated even at 3 mM, thus reflecting at least the Ca^{2+}-dependent and rate-limiting process; *i.e.* the lumenal Ca^{2+}-induced change from *E*2P to *E*2PCa_2. This reverse transition rate in the wild type in the presence of K^+ was significantly faster than those in the wild type in the absence of K^+ and in Y122A (as well as in the other Y122-HC mutants (Supplemental Figure 3) especially at the high Ca^{2+} concentration over 1 mM.

Here it is also interesting to note that the affinity of *E*2P for the lumenal Ca^{2+} in the wild type without K^+ and the Y122-HC mutants is significantly higher than in the wild type with K^+ (see Fig. 8*B*). If the rate of lumenal Ca^{2+} access and binding to *E*2P is solely slowed in the wild type without K^+ and Y122-HC mutants, a decrease in the affinity is rather the consequence, which is in contrast to the observed increase. Therefore the rates of the Ca^{2+} release from *E*2PCa_2 in the wild type without K^+ and in the Y122-HC mutants are also presumably retarded significantly as compared with that in the wild type in the presence of K^+. Namely, the mutations of Y122-HC and the lack of K^+ binding affect the energy levels of Ca^{2+}-free and -bound *E*2P states and also that of the transition state for lumenal gating (opening), and favor the Ca^{2+}-bound state *E*2PCa_2 and the closed lumenal gate.

DISCUSSION

Roles of Y122-HC in Ca^{2+}-release from E2PCa_2 and in E2P Hydrolysis — In this study, we found that the mutations of any of the seven residues in Y122-HC increase the lumenal Ca^{2+} affinity and retard the lumenal Ca^{2+} access to the transport sites in *E*2P. These mutations also retard markedly the hydrolysis of the Ca^{2+}-released form of *E*2P (22, 23). Thus, the proper formation of Y122-HC from the seven residues is critical for both Ca^{2+} release into lumen from *E*2PCa_2 (reducing the Ca^{2+} affinity and opening the lumenal gate), and formation of the *E*2P catalytic site for the subsequent Asp^{351}-acylphosphate hydrolysis. The formation of Y122-HC therefore functions critically for realizing and stabilizing the compactly organized and thus distorted structure of the Ca^{2+}-released form of *E*2P. The stabilization of this state is certainly important for making the time period long enough for Ca^{2+} release into lumen and likely for proton bindings to the empty Ca^{2+} sites, and for the fine rearrangement of the catalytic site for the subsequent Asp^{351}-acylphosphate hydrolysis.

As shown in Fig. 10 and Supplemental Figure 4, the extents of the mutational effects on the lumenal Ca^{2+} affinities and on the *E*2P hydrolysis rates varied significantly among the seven Y122-HC mutants, and depended on their positions. The residues of which mutation exhibited strongest effects on increasing the lumenal Ca^{2+} affinity were Leu^{119}, Tyr^{122}, and Leu^{180}. This agrees with the critical role of M2 for rearrangement of the transmembrane helices for the Ca^{2+}-release; *i.e.* the tight association of the top part of M2 with the largely rotating A domain in Y122-HC functions for the lever-like inclination of M2 to push the lumenal part of M4 to open the

lumenal gate (14). In fact, in $E2PCa_2$ trapped by the elongation of the A/M1-linker, the Leu^{119}/Tyr^{122} region on the top part of M2 is not involved fully in Y122-HC (9).

The residues of which mutations exhibited the strongest retardation of the *E*2P hydrolysis were Ile^{232} at the top part of the A/M3-linker and, again, Leu^{119} and Tyr^{122} on the A/M2-linker (top part of M2). Thus these residues on the linkers seem to contribute most critically to produce the proper configuration of the catalytic site. Consistently, the proteolytic cleavage at Leu^{119} on the A/M2-linker causes a marked inhibition of the *E*2P hydrolysis (43). The structural changes producing the Ca^{2+} release may be transmitted to the catalytic site *via* these residues of Y122-HC on the linkers, thereby ensuring the *E*2P hydrolysis to occur after the Ca^{2+} release. In any case, the different degree of the contributions of the seven residues of Y122-HC to the Ca^{2+} release and subsequent formation of the *E*2P catalytic site may suggest a possible sequential gathering of the seven residues. This possibility will be discussed more in the last section of "DISCUSSION" in relation to the crystal structure $E2{\cdot}BeF_3^-$ (17, 18).

Structural Mechanism Involving Y122-HC and Other Critical Elements — In $E1Ca_2{\cdot}AlF_4^-{\cdot}ADP \rightarrow E2{\cdot}MgF_4^{2-}$ as an overall structural change including the *E*P isomerization and Ca^{2+} release (Supplemental Figure 5A), the A domain largely rotates and M2 largely inclines. Also the P domain markedly inclines toward the underneath of the A domain, and rotates by approximately 20º around the phosphorylation site (Asp^{351}) parallel to the membrane and in the opposite direction of the A-domain rotation. These motions involve (can be dissected into) the horizontal and vertical factors, parallel and perpendicular to the membrane plane. As a consequence of the motions, the A and P domains and M2 will come to their appropriate positions producing their tight association at Y122-HC. At the A-P domain interface in the *E*2P analog structures, there is another interaction network between these domains at the Val^{200} loop, Asp^{196}-Asp^{203} of the A domain (Fig. 1, and see Supplemental Figure III in Ref. 23 for the details of the interactions and central role of Val^{200}). Our previous mutations of Val^{200} showed (24) that this A-P domain interaction is critical for Ca^{2+} release from $E2PCa_2$ and for formation of the *E*2P catalytic site, thus very similarly to Y122-HC. Then note that in the *E*2P analog structures (see Supplemental Figure 5A for $E2{\cdot}MgF_4^{2-}$), the two networks at Y122-HC and at Val^{200} are located at each side of the A-P domain interface on its *Top view* and at the bottom and upper parts of the interface, respectively on its *Side view*. Thus the two are situated horizontally and vertically with the specific relative positioning. It is very likely that this positioning of the two is most efficiently functioning to realize and stabilize the compactly organized and distorted structure of the Ca^{2+}-released *E*2P: *i.e.* the interactions at the two positions are most appropriate to produce the horizontal and vertical motions of the P and A domains and M2 required for Ca^{2+} release from $E2PCa_2$, and to stabilize the Ca^{2+}-released *E*2P state. Certainly these motions cause the rearrangements in the transmembrane helices for Ca^{2+} release: *e.g.* the P-domain inclination with slight rotation is directly associated with the bending and slight rotation of connected M4/M5 and downward movement of M4, thus their twisting-like motion. The largely inclining M2 pushes the lumenal part of M4 (Supplemental Figure 5B). Hence the Ca^{2+} sites are destroyed and lumenal gate is opened.

It should be noted that, for the loss of the ADP-sensitivity $E1PCa_2 \rightarrow E2PCa_2$, the large rotation of the A domain and its docking onto the P domain should occur so as to bring the T^{181}GES loop above Asp^{351}-acylphosphate to block the ADP access from the N domain. As the motive force of this large A-domain rotation approximately parallel to membrane plane, the strain imposed on the A/M3-linker in $E1PCa_2$ was predicted to be critical (13, 14, 20, 44). Also, the sufficiently long length of the A/M1-linker was revealed to be critical for this *E*P isomerization, in this case, probably for realizing the $E2PCa_2$ structure, in which the A domain is positioned above the P domain (9, 45). For the subsequent Ca^{2+} release in $E2PCa_2 \rightarrow E2P + 2Ca^{2+}$, the A/M1-linker with its appropriately short length (therefore its strain) is critical (9): Actually, the elongation of this linker blocks completely Ca^{2+}-deocclusion/release from $E2PCa_2$, thus traps this $E2PCa_2$ state, in which Y122-HC is not properly formed yet in contrast to its proper formation in the Ca^{2+}-released form of *E*2P with the lumenally opened normal Ca^{2+} release pathway (9). The results clearly demonstrated that the native and appropriately short length of A/M1-linker functions critically in inducing the motions from the $E2PCa_2$ state, especially inclination of the A and P domains and M2, to accomplish the Y122-HC formation and the Ca^{2+}-deocclusion/release from $E2PCa_2$. During the Y122-HC formation, the interaction-force

being produced in Y122-HC will likely function to induce final process of the vertical and horizontal motions of the P and A domain and M2 to realize and stabilize the Ca^{2+}-released *E*2P structure (Supplemental Figure 6). Importantly also, the *E*2P catalytic site is produced by these rearrangements. In this mechanism, a possible hydrolysis of Asp^{351}-acylphosphate without releasing Ca^{2+} will be avoided; thereby the ordered reaction sequence of the Ca^{2+} release from $E2PCa_2$ and the subsequent *E*2P hydrolysis will be accomplished for the energy coupling.

Possible Structural Role of K^+ for Reducing Ca^{2+} Affinity and Lumenal Gating — K^+ is known to markedly accelerate the *E*2P hydrolysis (35, 36), and also to modulate the *E*2 to $E1Ca_2$ transition in the non-phosphorylated Ca^{2+}-ATPase (46, 47). In the present study, we further found that the K^+ binding is important for reducing the affinity for Ca^{2+} and lumenal gating thus for Ca^{2+} release from $E2PCa_2$. In the crystal structure $E1Ca_2{\cdot}AlF_4^-{\cdot}ADP$, K^+ is situated at the bottom part of the P domain and coordinated by the backbone carbonyls of the loop Leu^{711}-Glu^{715} and by the Glu^{732} side chain (Fig. 11). The K^+ binding at this site was indeed previously found by the mutations to be critical for the stimulation of the *E*2P hydrolysis (37). In the structures *E*2P analogs and *E*2(TG), this K^+ site of the P domain comes very close to the A/M3-linker, and actually K^+ at this site is further coordinated by the Gln^{244} side chain on the A/M3-linker (see $E2{\cdot}AlF_4^-$ in Fig. 11). Since the alanine-substitution of Gln^{244} and those of Glu-Gln-Asp^{245} gave virtually no effect on Ca^{2+} transport activity (48), K^+ at this region may be coordinated by their neighboring residues or backbone carbonyls on the A/M3-linker and thereby play structural function. In the present study, we found that the lack of K^+ binding have the consequences very similar to those of the mutations at Y122-HC. It is therefore possible that the K^+ binding functions with similar structural effects as Y122-HC to produce the proper structure of the Ca^{2+}-released form of *E*2P.

Then note that the K^+ site of the P domain in $E1Ca_2{\cdot}AlF_4^-{\cdot}ADP$ is situated at much higher position from the membrane plane than the Gln^{244} region on the A/M3-linker (Fig. 11) and that, in the change $E1Ca_2{\cdot}AlF_4^-{\cdot}ADP \rightarrow E2{\cdot}AlF_4^-$ (or $E2{\cdot}BeF_3^-$ and $E2{\cdot}MgF_4^{2-}$), the P domain with connected M4/M5 largely inclines toward the A domain, hence the K^+ site with bound K^+ on the P domain moves down to the Gln^{244} region on the A/M3-linker to contact with. The interactions between the bottom part of the P domain and the A/M3-linker *via* bound K^+ thus produced would likely cross-link them and hence contribute to formation and stabilization of this compactly organized Ca^{2+}-released structure of *E*2P with the reduced Ca^{2+} affinity and lumenally opened gate. Alternatively, it is also possible that the appropriate P-domain structure produced by K^+ binding on this domain solely contributes to the formation of the Ca^{2+}-released *E*2P structure.

Y122-HC in Crystal Structure of $E2{\cdot}BeF_3^-$ — The crystal structures of $E2{\cdot}BeF_3^-$, the analog for the *E*2P ground state (21), were solved at atomic level very recently with and without bound thapsigargin, TG ($E2BeF_3^-$ and $E2BeF_3^-$(TG) (17, 18)). Surprisingly, in this crystallized $E2{\cdot}BeF_3^-$, the side chains of Ile^{119} and Tyr^{122} are somewhat pointing away from the clustered other five residues on the A and P domains (Ile^{179}/Leu^{180}/Ile^{232} and Val^{705}/Val^{726}), although all these seven residues are closely located in the $E2{\cdot}BeF_3^-$ structures of both 2ZBE (17) and 3B9B (18). On the other hand, Y122-HC is formed fully from all these seven residues in $E2BeF_3^-$(TG) as well as in the other *E*2P analogous structures, $E2{\cdot}AlF_4^-$ and $E2{\cdot}MgF_4^{2-}$. Thus, the assembling manner of the seven residues in the crystal structure $E2{\cdot}BeF_3^-$ seemingly conflicts somehow with our results that the gathering of all the seven residues including Tyr^{122}/Ile^{119} in Y122-HC is required for producing the Ca^{2+}-released *E*2P. Furthermore, Tyr^{122} and Ile^{119} on the top part of M2 (A/M2-linker) are likely most critical in Y122-HC and play central roles (Fig. 10). Our previous biochemical structural analysis of SR Ca^{2+}-ATPase in solution by the proteolysis and the lumenal Ca^{2+} accessibility demonstrated (21) that in $E2{\cdot}BeF_3^-$ without TG, Leu^{119}/Tyr^{122} are surely gathered and involved in Y122-HC, and thereby the lumenal gate is opened and the lumenal Ca^{2+} is accessible to the transport sites. Thus the crystal structure $E2{\cdot}BeF_3^-$ seems to conflict also with these biochemical results obtained in solution.

Nevertheless, as a comprehensive idea, the crystal structure of $E2{\cdot}BeF_3^-$ may be consistent with (or indicative of) the view that the gathering of the seven residues to form Y122-HC upon motions of the A and P domains and M2 (A/M2-linker) occurs in some ordered sequence but not necessarily at once (see Fig. 10 and its related "DISCUSSION"). Most peculiar to us is that Tyr^{122} and Leu^{119}, of which mutations exhibited the most inhibitory effects, are not involved yet in the hydrophobic

cluster in the crystal structures $E2{\cdot}BeF_3^-$. Then here note that in the structures $E2{\cdot}BeF_3^-$, a Mg^{2+} ion is bound near the Ca^{2+} binding sites in the transmembrane domain as in extremely high Mg^{2+} concentration employed for crystallization (18) or protonation on the residues of transmembrane helices including Ca^{2+} ligands must have been occurred as in low pH for crystallization (17). Thus, these ligations are probably involved critically in the stabilization of the transmembrane helices for the crystallization. This might mean that the transmembrane structure thus stabilized differs from that without any ligations, *i.e.* the state immediate after the Ca^{2+} release (the empty Ca^{2+} sites) that is realized by the contribution of Y122-HC. Therefore, Y122-HC is, in return, disrupted or not properly produced yet in the crystal structure $E2{\cdot}BeF_3^-$ as if it occurs with the lumenal Ca^{2+} binding in the $E2PCa_2$ state as postulated in this study. Therefore the following sequential gathering of the seven residues to produce Y122-HC can be speculated: The five hydrophobic residues on the A domain (Ile^{179}/Leu^{180}/Ile^{232}) and P domain (Val^{705}/Val^{726}) are first gathered upon the motions of the A and P domains and top part of M2 (A/M2-linker), and subsequently, the top part of M2 including Ile^{119} and Tyr^{122} takes further motions during the final process of the M2-inclination to join them and produce the fully assembled Y122-HC, thereby to realize and stabilize fully the gathered state of the A and P domains and top part of M2 (A/M2-linker) as in the Ca^{2+}-released form of *E*2P. Being in agreement with this view, in $E2PCa_2$ trapped by the elongation of the A/M1-linker, Leu^{119}/Tyr^{122} on the top part of M2 is not fully involved yet in Y122-HC (9). The Ca^{2+}-released and empty Ca^{2+} sites (without any protonation and stabilization immediately after the Ca^{2+} release) will be subsequently protonated producing the *E*2P ground state for its hydrolysis.

Alternatively, if a possible contribution of such ligation in the transmembrane domain (Mg^{2+} or protonation) should not be concerned in the crystallization of $E2{\cdot}BeF_3^-$, the followings might be possible: First of all, the arrangements of helices of the Ca^{2+}-released empty transport sites must be unstable, for example, due to possible repulsions between the negative charges of the Ca^{2+} ligands. Then to relieve the instability, the most effective gathering of Tyr^{122}/Leu^{119} in Y122-HC, which produces and stabilizes the Ca^{2+}-released empty state, might possibly be disrupted, thereby the helices may be rearranged so as to form the more stabilized arrangements that can be crystallized.

Acknowledgments — We would like to thank Dr. David H. MacLennan, University of Toronto, for his generous gift of SERCA1a cDNA and Dr. Randal J. Kaufman, Genetics Institute, Cambridge, MA, for his generous gift of the expression vector pMT2. We are also grateful to Dr. Chikashi Toyoshima, University of Tokyo, for helpful discussions.

REFERENCES

1. Hasselbach, W., and Makinose, M. (1961) *Biochem. Z.* **333,** 518-528
2. Ebashi, S., and Lipmann, F. (1962) *J. Cell Biol.* **14,** 389-400
3. Inesi, G., Sumbilla, C., and Kirtley, M. E. (1990) *Physiol. Rev.* **70,** 749-776
4. Møller, J. V., Juul, B., and le Maire, M. (1996) *Biochim. Biophys. Acta* **1286,** 1-51
5. MacLennan, D. H., Rice, W. J., and Green, N. M. (1997) *J. Biol. Chem.* **272,** 28815-28818
6. McIntosh, D. B. (1998) *Adv. Mol. Cell Biol.* **23A,** 33-99
7. Toyoshima, C., and Inesi, G. (2004) *Annu. Rev. Biochem.* **73,** 268-292
8. Toyoshima, C. (2008) *Arch. Biochem. Biophys.* doi 10.1016/j.abb.2008.04.017
9. Daiho, T., Yamasaki, K., Danko, S., and Suzuki, H. (2007) *J. Biol. Chem.* **282,** 34429-34447
10. Toyoshima, C., Nakasako, M., Nomura, H., and Ogawa, H. (2000) *Nature* **405,** 647-655
11. Toyoshima, C., and Nomura, H. (2002) *Nature* **418,** 605-611
12. Sørensen, T. L-M., Møller, J. V., and Nissen, P. (2004) *Science* **304,** 1672-1675
13. Toyoshima, C., and Mizutani, T. (2004) *Nature* **430,** 529-535
14. Toyoshima, C., Nomura, H., and Tsuda, T. (2004) *Nature* **432,** 361-368
15. Olesen, C., Sørensen, T. L.-M., Nielsen, R. C., Møller, J. V., and Nissen, P. (2004) *Science* **306,** 2251-2255
16. Takahashi, M., Kondou, Y., and Toyoshima, C. (2007) *Proc. Natl. Acad. Sci. U. S. A.* **104,** 5800-5805

17. Toyoshima, C., Norimatsu, Y., Iwasawa, S., Tsuda, T., and Ogawa, H. (2007) *Proc. Natl. Acad. Sci. U. S. A.* **104**, 19831-19836
18. Olesen, C., Picard, M., Winther, A.-M. L., Gyrup, C., Morth, J. P., Oxvig, C., Møller, J. V., Nissen, P. (2007) *Nature* **450**, 1036-1042.
19. Danko, S., Daiho, T., Yamasaki, K., Kamidochi, M., Suzuki, H., and Toyoshima, C. (2001) *FEBS Lett.* **489,** 277–282
20. Danko, S., Yamasaki, K., Daiho, T., Suzuki, H., and Toyoshima, C. (2001) *FEBS Lett.* **505,** 129-135
21. Danko, S., Yamasaki, K., Daiho, T., and Suzuki, H. (2004) *J. Biol. Chem.* **279,** 14991-14998
22. Yamasaki, K., Daiho, T., Danko, S., and Suzuki, H. (2004) *J. Biol. Chem.* **279,** 2202-2210
23. Wang, G., Yamasaki, K., Daiho, T., and Suzuki, H. (2005) *J. Biol. Chem.* **280,** 26508-26516
24. Kato, S., Kamidochi, M., Daiho, T., Yamasaki, K., Wang, G., and Suzuki, H. (2003) *J. Biol. Chem.* **278,** 9624-9629
25. Kaufman, R. J., Davies, M. V., Pathak, V. K., and Hershey, J. W. B. (1989) *Mol. Cell. Biol.* **9,** 946-958
26. Maruyama, K., and MacLennan, D. H. (1988) *Proc. Natl. Acad. Sci. U. S. A.* **85,** 3314-3318
27. Kanazawa, T., Saito, M., and Tonomura, Y. (1970) *J. Biochem*. (*Tokyo*) **67,** 693-711
28. Weber, K., and Osborn, M. (1969) *J. Biol. Chem.* **244,** 4406-4412
29. Daiho, T., Suzuki, H., Yamasaki, K., Saino, T., and Kanazawa, T. (1999) *FEBS Lett.* **444,** 54-58
30. Lowry, O. H., Rosebrough, N. J., Farr, A. L., and Randall, R. J. (1951) *J. Biol. Chem.* **193,** 265-275
31. Humphrey, W., Dalke, A., and Schulten, K. (1996) *J. Mol. Graphics* **14,** 33-38
32. Coan, C., Verjovski-Almeida, S., and Inesi, G. (1979) *J. Biol. Chem.* **254,** 2968-2974
33. Prager, R., Punzengruber, C., Kolassa, N., Winkler, F., and Suko, J. (1979) *Eur. J. Biochem.* **97,** 239-250
34. de Meis, L., and Inesi, G. (1982) *J. Biol. Chem.* **257,** 1289-1294
35. Shigekawa, M., and Pearl, L. J. (1976) *J. Biol. Chem.* **251,** 6947-6952
36. Shigekawa, M., and Dougherty, J. P. (1978) *J. Biol. Chem.* **253,** 1451-1457
37. Sørensen, T. L-M., Clausen, J. D., Jensen, A.-M. L., Vilsen, V., Møller, J. V., Andersen, J. P., and Nissen, P. (2004) *J. Biol. Chem.* **279,** 46355-46358
38. de Meis, L., Martins, O. B., and Alves, E. W. (1980) *Biochemistry* **19,** 4252-4261
39. Fersht, A. R. (1999) *Structure and Mechanism in Protein Science: A Guide to Enzyme Catalysis and Protein Folding*, pp. 132-168, W. H. Freeman and Co., New York
40. Sato, K., Yamasaki, K., Daiho, T., Miyauchi, Y., Takahashi, H., Ishida-Yamamoto, A., Nakamura, S., Iizuka, H., and Suzuki, H. (2004) *J. Biol. Chem.* **279,** 35595-35603
41. Shigekawa, M., Wakabayashi, S., and Nakamura, H. (1983) *J. Biol. Chem.* **258,** 8698-8707
42. Wakabayashi, S., and Shigekawa, M. (1987) *J. Biol. Chem.* **262,** 11524-11531
43. Lenoir, G., Picard, M., Gauron, C., Montigny, C., Le Maréchal, P., Falson, P., le Maire, M., Møller, J.V., and Champeil, P. (2004) *J. Biol. Chem.* **279,** 9156-9166
44. Møller, J.V., Lenoir, G., Marchand, C., Montigny, C., le Maire, M., Toyoshima, C., Juul, B. S., and Champeil, P. (2002) *J. Biol. Chem.* **277,** 38647-38659
45. Daiho, T., Yamasaki, K., Wang, G., Danko, S., and Suzuki, H. (2003) *J. Biol. Chem.* **278,** 39197-39204
46. Lee, A. G., Baker, K., Khan, Y. M., and East, J. M. (1995) *Biochem. J.* **305**, 225-231
47. Champeil, P., Henao, F., and de Foresta, B. (1997) *Biochemistry* **36,** 12383-12393
48. Clarke, D. M., Maruyama, K., Loo, T. W., Leberer, E., Inesi, G., and MacLennan, D. H. (1989) *J. Biol. Chem.* **264,** 11246-11251

FOOTNOTES

*This work was supported by a Grant-in-Aid for Scientific Research (C) (to K.Y.) and (B) (to H.S.) from the Ministry of Education, Culture, Sports, Science and Technology of Japan.

[1]The abbreviations used are: SERCA1a, adult fast-twitch skeletal muscle sarcoplasmic reticulum Ca^{2+}-ATPase; *E*P, phosphoenzyme; *E*1P, ADP-sensitive phosphoenzyme; *E*2P, ADP-insensitive phosphoenzyme; MOPS, 3-(*N*-morpholino) propanesulfonic acid; TG, thapsigargin; Y122-HC, Tyr^{122}-hydrophobic cluster.

[2]Maximal level of the ADP-insensitive *E*P of L180A at the low Ca^{2+} concentrations (44% of total amount of *E*P) was significantly lower than those of the other mutants. It may be due to the significantly faster *E*2P hydrolysis rate in L180A as compared with the rates in the others, as shown in Supplemental Figure 4.

[3]Its slope was approximately 0.2 $s^{-1}mM^{-1}$ at 0~2 mM Ca^{2+}. In Fig. 3, the rate of the forward *E*1PCa_2 to *E*2P conversion was estimated to be 0.02 s^{-1}. Therefore the calculation with these values, 0.02 s^{-1} divided by 0.2 $s^{-1}mM^{-1}$, gave the apparent affinity for lumenal Ca^{2+} in *E*2P of Y122A as 100 μM. This value agreed very well with that (160 μM) obtained in Fig. 2 under the same conditions (pH 7.3) at the steady state.

[4]As a possible reason for the less steep Ca^{2+}-dependent curve observed with I232A and V705A over ~1 mM, it might be possible that the rate in the transition from *E*2PCa_2 to *E*1PCa_2 is slower in these mutants than in the other mutants, and this step became a rate-limiting at the high Ca^{2+} concentrations where the lumenal Ca^{2+}-induced change to *E*2PCa_2 became fast.

FIGURE LEGENDS

FIGURE 1. **Structure of SERCA1a and formation of Tyr^{122}-hydrophobic cluster.** The coordinates for the structures *E*1Ca_2·AlF_4^-·ADP, (the analog for the transition state of the phosphoryl transfer *E*1~PCa_2·ADP, *left panel*) and *E*2·MgF_4^{2-} (*E*2·P_i analog (21), *right panel*) of Ca^{2+}-ATPase were obtained from the Protein Data Bank (PDB accession code 1T5T and 1WPG, respectively (12, 14)). The arrows indicate approximate movements of the A and P domain and the top part of M2 (Leu^{119}/Tyr^{122}) in the change from *E*1·AlF_4^-·ADP to *E*2·MgF_4^{2-}. The seven hydrophobic residues, Ile^{179}/Leu^{180}/Ile^{232} on the A domain, Leu^{119}/Tyr^{122} on the A/M2-linker, Val^{705}/Val^{726} on the P domain are depicted as van der Waals spheres. They gather to form a hydrophobic cluster around Tyr^{122} in the change *E*1Ca_2·AlF_4^-·ADP → *E*2·MgF_4^{2-} (Y122-HC, surrounded by *red dotted circle*). The top part of M2 including Leu^{119}/Tyr^{122} is unwound in *E*2·MgF_4^{2-}, *E*2·AlF_4^-, and *E*2·BeF_3^- with bound thapsigargin (TG), thus becomes the A/M2-linker loop (see the region of M2 colored by *pink*).

FIGURE 2. **Ca^{2+} dependence of accumulation of ADP-insensitive *E*P in the steady state in mutant Y122A.** Microsomes expressing the mutant Y122A were phosphorylated with [γ-^{32}P]ATP at various Ca^{2+} concentrations and pHs as indicated at 0 °C for 5 min in a mixture containing 20 μg/ml microsomal protein, 50 mM MOPS/Tris, 0.1 M KCl, 7 mM $MgCl_2$, 0.01 mM EGTA, 3 μM A23187, 10 μM [γ-^{32}P]ATP, and various concentrations of $CaCl_2$. For the determination of the accumulated ADP-insensitive *E*P, an equal volume (50 μl) of a mixture containing 10 mM ADP, 7 mM $MgCl_2$, 10 mM EGTA, 50 mM MOPS/Tris (pH 6.8, 7.3, or 7.8 as indicated), and 0.1 M KCl was added to the above phosphorylation mixture. At 1 s after this addition, the reaction was quenched with trichloroacetic acid. ADP-sensitive *E*P disappeared entirely within 1 s after the addition of ADP. The total amounts of *E*P were nearly the same under all the conditions (data not shown). The amount of ADP-insensitive *E*P is shown as a percentage of the total amount of *E*P. *Solid lines* show the least squares fit to the Hill equation. Apparent Ca^{2+} affinities and Hill coefficients thus obtained were 360 μM and 2.1 (pH 6.8), 160 μM and 1.9 (pH 7.3), and 76 μM and 2.0 (pH 7.8).

FIGURE 3. **Time course of the change in the fraction of ADP-insensitive *E*P upon Ca^{2+}-concentration jump.** Microsomes expressing the mutant Y122A (20 μg/ml) were phosphorylated with [γ-^{32}P]ATP at pH 7.3 for 5 min in the presence of 10 μM (○) or 1 mM $CaCl_2$ (●) without EGTA in the phosphorylation solution otherwise as described in Fig. 2. Then an equal volume of the solution containing 2 mM $CaCl_2$ or 2 mM EGTA (otherwise as in the phosphorylation solution) was added to give final free Ca^{2+} concentrations 1 mM and 80 nM, respectively. At the indicated times after this Ca^{2+} jump, the total amount of *E*P and the amount of ADP-insensitive *E*P was determined as in Fig. 2. *Solid lines* show the least squares fit to a single exponential. The total amount of *E*P was not changed during the period of observation in both cases (data not shown). The amount of ADP-insensitive *E*P is shown as a percentage of the total amount of *E*P.

FIGURE 4. **Effect of calcium ionophore on the Ca^{2+} dependence of ADP-insensitive *E*P accumulation in the steady state.** Microsomes expressing the mutant Y122A (20 μg/ml) were phosphorylated at 0 °C for 5 min in the medium containing 50 mM MOPS/Tris (pH 7.3), 0.1 M KCl, 7 mM $MgCl_2$, 10 μM $CaCl_2$, 10 μM [γ-^{32}P]ATP, and 50 μM Ruthenium Red (to block Ca^{2+} channels as much as possible) in the presence (○) or absence (●) of 3 μM A23187. Then the free Ca^{2+} concentration was changed as indicated on abscissa by mixing with an equal volume of a solution containing 50 mM MOPS/Tris (pH 7.3), 0.1 M KCl, 7 mM $MgCl_2$, 2 mM EGTA, and various concentrations of $CaCl_2$. After 10 s of this Ca^{2+} jump, the total amount of *E*P and the fraction of the ADP-insensitive *E*P were determined as described in Fig. 2. The inclusion of Ruthenium Red in the presence of A23187 caused a slight decrease in the ADP-insensitive *E*P fraction at the Ca^{2+} concentrations below ~100 μM (*cf.* Fig. 2) for unknown reasons.

FIGURE 5. **Ca^{2+} dependence of accumulation of ADP-insensitive *E*P in mutants for Tyr^{122}-hydrophobic cluster.** Microsomes expressing each of the seven Y122-HC mutants (indicated in the figure) were phosphorylated with [γ-^{32}P]ATP at various concentrations of Ca^{2+} and pH 7.3, otherwise as described in Fig. 2. *Solid lines* show the least squares fit to the Hill equation. The fitting parameters including the apparent Ca^{2+} affinity and the Hill coefficient thus obtained were listed in Table 1.

FIGURE 6. **Ca^{2+} dependence of accumulation of ADP-insensitive *E*P in the absence of K^+.** Microsomes expressing the wild type (*A*) or Y122A (*B*) SERCA1a were phosphorylated with [γ-^{32}P]ATP at various Ca^{2+} concentrations and pH (6.8 (○), 7.3 (●), and 7.8 (Δ)) in the presence of 0.1 M LiCl in place of KCl otherwise under the exactly same conditions as those described in Fig. 2. The amount of ADP-insensitive *E*P was determined by the addition of the ADP solution that contains 0.1 M LiCl in place of KCl otherwise as in Fig. 2. The total amount of *E*P was nearly constant under all the conditions (data not shown). The amount of ADP-insensitive *E*P is shown as a percentage of the total amount of *E*P. *Solid lines* show the least squares fit to the Hill equation. Apparent Ca^{2+} affinities and Hill coefficients thus obtained with the wild type (*panel A*) were 930 μM and 1.8 (pH 6.8), 400 μM and 1.5 (pH 7.3), and 310 μM and 1.9 (pH 7.8), and those obtained with Y122A (*panel B*) were 1000 μM and 1.9 (pH 6.8), 220 μM and 2.2 (pH 7.3), and 130 μM and 1.7 (pH 7.8).

FIGURE 7. **Lumenal Ca^{2+}- and ADP-induced reverse *E*2P decay of Y122A in the presence of K^+.** *A*, microsomes (100 μg/ml) expressing the mutant Y122A were phosphorylated with $^{32}P_i$ for 10 min at room temperature in the absence of Ca^{2+} in a medium containing 50 mM MOPS/Tris (pH 7.3), 7 mM $MgCl_2$, 1 mM EGTA, 15 μM A23187, 0.1 mM $^{32}P_i$, and 20% Me_2SO (that favors extremely the *E*2P formation (38)), and then the reaction mixture was chilled on ice. Subsequently, the phosphorylated sample was diluted at 0 °C with a 20-fold volume of a chase solution containing 50 mM MOPS/Tris (pH 7.3), 105 mM KCl, 7 mM $MgCl_2$, 1 mM EGTA, 0.1mM non-radioactive P_i and 0.105 mM ADP without or with various concentrations of $CaCl_2$ to give the final free Ca^{2+} concentrations as indicated. At the indicated periods, the chase reaction was terminated by trichloroacetic acid and the amount of *E*P was determined. *Solid lines* show the least squares fit to a single exponential decay. The decay rates thus obtained were plotted *versus* the Ca^{2+} concentration in *panel B*.

FIGURE 8. **Lumenal Ca^{2+}- and ADP-induced reverse *E*2P decay of wild type and Y122A in the absence and presence of K^+.** *A*, microsomes (100 μg/ml) expressing wild type (WT) or Y122A were phosphorylated with $^{32}P_i$ in the presence of A23187 and absence of Ca^{2+}, and then chilled on ice, as described in Fig. 7. Subsequently, the phosphorylated sample was diluted at 0 °C with a 20-fold volume of a chase solution containing non-radioactive P_i, various concentrations of $CaCl_2$, and ADP in the presence of 105 mM KCl (*open symbols*) or 105 mM LiCl in place of KCl (*closed symbols*), otherwise as described in Fig. 7. The time courses of *E*P decay were fitted to single exponential (data not shown, see Fig. 7*A* as an example). The rates thus obtained were plotted *versus* the Ca^{2+} concentrations. *B*, the fraction ADP-insensitive *E*P (F_{E2P}) in the total amount of *E*P at steady state was simulated by using the rate of *E*2P decay (v_2) and the rate of the *E*1PCa_2 to *E*2P isomerization (loss of ADP-sensitivity, v_1) with an equation $F_{E2P} = v_1/(v_1 + v_2)$. Here, v_2 is the *E*2P decay rate obtained above in *panel A* at each Ca^{2+} concentrations. The v_1 was obtained as described in Fig. 3 by the Ca^{2+} jump experiments from high (1 mM) to low (80 nM, virtually Ca^{2+} removal) for Y122A with 0.1 M K^+ or Li^+ (without K^+) and for the wild type with 0.1 M Li^+ (without K^+). For the wild type with 0.1 M K^+, the forward decay rate of *E*1PCa_2 formed from ATP was used as the v_1 value, because the *E*1PCa_2 to *E*2P transition (the loss of ADP-sensitivity) is rate-limiting for the *E*1PCa_2 decay *via* *E*2P and its

subsequent rapid hydrolysis. The v_1 values actually used for the calculation were 0.049 s^{-1} (wild type with K^+), 0.071 s^{-1} (wild type with Li^+), 0.021 s^{-1} (Y122A with K^+), and 0.034s^{-1} (Y122A with Li^+). The fraction of ADP-insensitive *E*P thus calculated was plotted *versus* the Ca^{2+} concentrations. The solid lines show the least squares fit to the Hill equation. In the *inset*, the ordinate is in a magnified scale for wild type with K^+. In Table 2, the affinities and the Hill coefficients of the wild type and the Y122-HC mutants thus "*Estimated by kinetic analyses*" in the absence and presence of K^+ at pH 7.3 are summarized together with those actually "*Determined by the steady-state analyses*" of the lumenal Ca^{2+}-induced change of the fraction of ADP-insensitive *E*P under otherwise the same conditions in Figs. 2 and 6.

FIGURE 9. **Kinetics of lumenal Ca^{2+}-induced change of *E*2P to *E*1PCa_2 in the wild type in the presence of K^+ without ADP.** *A*, the microsomes expressing the wild type were phosphorylated with $^{32}P_i$ in the presence of A23187 and absence of Ca^{2+} and chilled on ice, as described in Fig. 7. Subsequently, the phosphorylated sample was mixed at 0 °C with a 20-fold volume of chase solution containing 105 mM KCl and various concentrations of $CaCl_2$ without ADP, otherwise as described in Fig. 7. The final free Ca^{2+} concentrations were indicated in the figure. At the indicated time periods after this addition, the chase reaction was terminated by trichloroacetic acid and the amount of *E*P was determined. *Solid lines* show the least squares fit to a double exponential decay. The *E*P remaining in the second and slow phase was all in the ADP-sensitive form (thus *E*1PCa_2, data not shown), and the first and rapid phase is the forward hydrolysis of *E*2P without bound Ca^{2+}. *B*, the fraction of *E*P in the second phase in the total amount of *E*P was obtained by extrapolating to the zero time in the double exponential decay fitting, and plotted *versus* the Ca^{2+} concentration. The data were fitted well with the Hill equation (*solid line*), and the Ca^{2+} concentration giving the 50% saturation and the Hill coefficient were found to be 750 μM and 1.5. Here note that the *E*P amount in the second phase is dependent on the ratio between the rate of the forward *E*2P hydrolysis and that of the reverse *E*2P to *E*1PCa_2 conversion upon the lumenal Ca^{2+} binding to *E*2P: The plot reflects the relative values between these forward and reverse rates of *E*2P rather than the lumenal Ca^{2+} affinity of *E*2P. *C*, by using the data obtained in *A* and *B* with the wild type in the presence of K^+, the rate of the lumenal Ca^{2+}-induced *E*1PCa_2 formation from *E*2P (k_{rev} (○)) was calculated at each Ca^{2+} concentration by the equation; $k_{rev} = k_h F_s/(1 - F_s)$. Here, F_s is the fraction of *E*P in the second phase, and k_h is the forward hydrolysis rate of *E*2P without Ca^{2+}. For comparison with the wild type in the absence of K^+ (●) and Y122A in the presence of K^+ (Δ), their lumenal Ca^{2+} access rates (the rates of the lumenal Ca^{2+}-induced reverse *E*2P decay *via* *E*1PCa_2 in the presence of ADP) obtained in Fig. 8*A* were plotted.

FIGURE 10. **Strength of the mutational effects of seven residues in Tyr^{122}-hydrophobic cluster on *E2*P hydrolysis and lumenal Ca^{2+} affinity.** The detailed structure at Y122-HC is shown with *E*2·AlF_4^- (the analog for *E*2~P, the transition state of the *E*2P hydrolysis (21), PDB code: 1XP5 (15)). The seven residues involved in Y122-HC (Tyr^{122}/Leu^{119}, Ile^{179}/Leu^{180}, Ile^{232}, and Val^{705}/Val^{726}), AlF_4^- bound at the phosphorylation site Asp^{351}, and the bound potassium ion are shown by van der Waals spheres. The seven residues in Y122-HC are colored differently based on the strength of the retardation of the *E*2P hydrolysis rate (*lower panel*) and that of the increase in the lumenal Ca^{2+} affinity (*upper panel*). The color changes gradually from *red* for strongest effects to *blue* as becoming weaker.

FIGURE 11. **Bound K^+ and Tyr^{122}-hydrophobic cluster in crystal structures.** The part of structures *E*1Ca_2·AlF_4^-·ADP (*E*1~PCa_2·ADP analog, *left*) and *E*2·AlF_4^- (*E*2~P analog, *right*) around Y122-HC and the bound K^+ ion are shown in cartoon models (PDB codes: 1T5T and 1XP5 (12, 15)). The two structures were manually aligned with M8-M10 helices, which do not move virtually in the two. K^+ bound in these structures is shown by *yellow* van der Waals sphere. Gln^{244} on the A/M3-linker at the immediate vicinity of the bound K^+ in *E*2·AlF_4^- is indicated by ball and stick model.

TABLE 1

Parameters obtained for Ca^{2+} dependence of accumulation of ADP-insensitive EP in Y122-HC mutants

As shown in Fig. 5, the lumenal Ca^{2+}-induced change in the steady-state accumulation of ADP-insensitive *E*P of the seven Y122-HC mutants in the presence of 0.1 M K^+ were fitted to the Hill equation. The parameters thus obtained by the least squares fit are listed here. $K_{0.5}$ is the Ca^{2+} concentration giving the half maximum change in the fraction of ADP-insensitive *E*P among the total amount of *E*P, therefore the apparent affinity for lumenal Ca^{2+}. The highest fraction of the ADP-insensitive *E*P at the low Ca^{2+} concentration range (0 ~ 10 μM) and its lowest fraction at the high Ca^{2+} concentration range (over ~mM) are also listed as the obtained parameters in the fitting (see Fig. 5). The value n_H is the Hill coefficient.

Mutant	Fraction of ADP-insensitive *E*P at highest and lowest Ca^{2+} concentration ranges		$K_{0.5}$	n_H
	High Ca^{2+}	Low Ca^{2+}		
	% of total amount of EP		*mM*	
L119A	11	78	0.12	2.1
Y122A	6	86	0.16	1.9
I179A	12	92	0.25	2.3
L180A	9	44	0.11	1.6
I232A	10	89	0.32	2.0
V705A	39	80	0.27	1.6
V726A	23	65	0.28	2.0

TABLE 2

Affinities of E2P for lumenal Ca^{2+} estimated by kinetic analyses and those determined at steady state analyses

As described in the Fig. 8*B*, the lumenal Ca^{2+}affinities ($K_{0.5}$) of *E*2P of the wild type and the mutant Y122A were estimated by the kinetic analyses of the lumenal Ca^{2+}-induced *E*2P to *E*1PCa_2 reverse transition and of the forward *E*1PCa_2 to *E*2P transition. The $K_{0.5}$ values and the Hill coefficients (n_H) thus estimated kinetically in Fig. 8 in the absence and presence of 0.1 M K^+ at pH 7.3 are summarized here. Listed together are those determined by the steady-state analyses of the lumenal Ca^{2+}-induced change in the accumulated fraction of the ADP-insensitive *E*P (*E*2P) under otherwise the same conditions in Figs. 2 and 6 for the mutant Y122A with and without K^+ and the wild type without K^+.

	K^+	Estimated by kinetic analyses		Determined by steady-state analyses	
	(0.1 M)	$K_{0.5}$	n_H	$K_{0.5}$	n_H
		mM		*mM*	
WT	+	1.48	2.2	-[a]	-[a]
	−	0.45	1.7	0.40	1.5
Y122A	+	0.15	1.9	0.16	1.9
	−	0.22	1.7	0.22	2.2

[a] Not determined because the accumulation of ADP-insensitive *E*P was very low at all the Ca^{2+} concentrations examined and therefore possible change was not revealed.

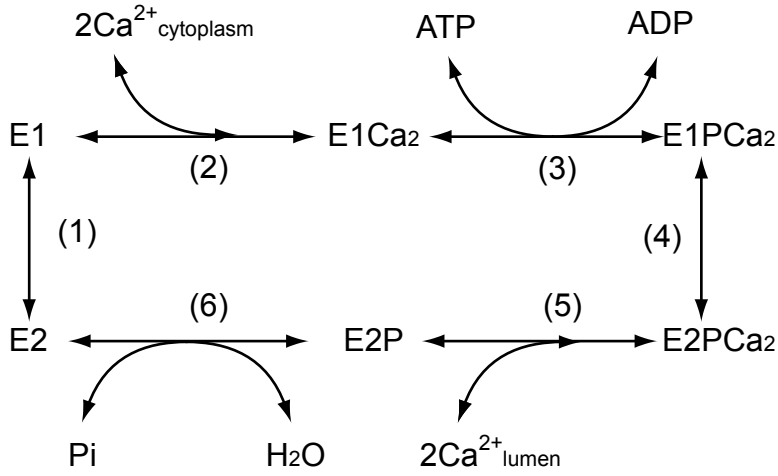
2Ca2+cytoplasm
ATP
ADP
E1
E1Ca2
E1PCa2
(2)
(3)
(1)
(4)
(6)
(5)
E2
E2P
E2PCa2
Pi
H2O
2Ca2+lumen

Scheme 1

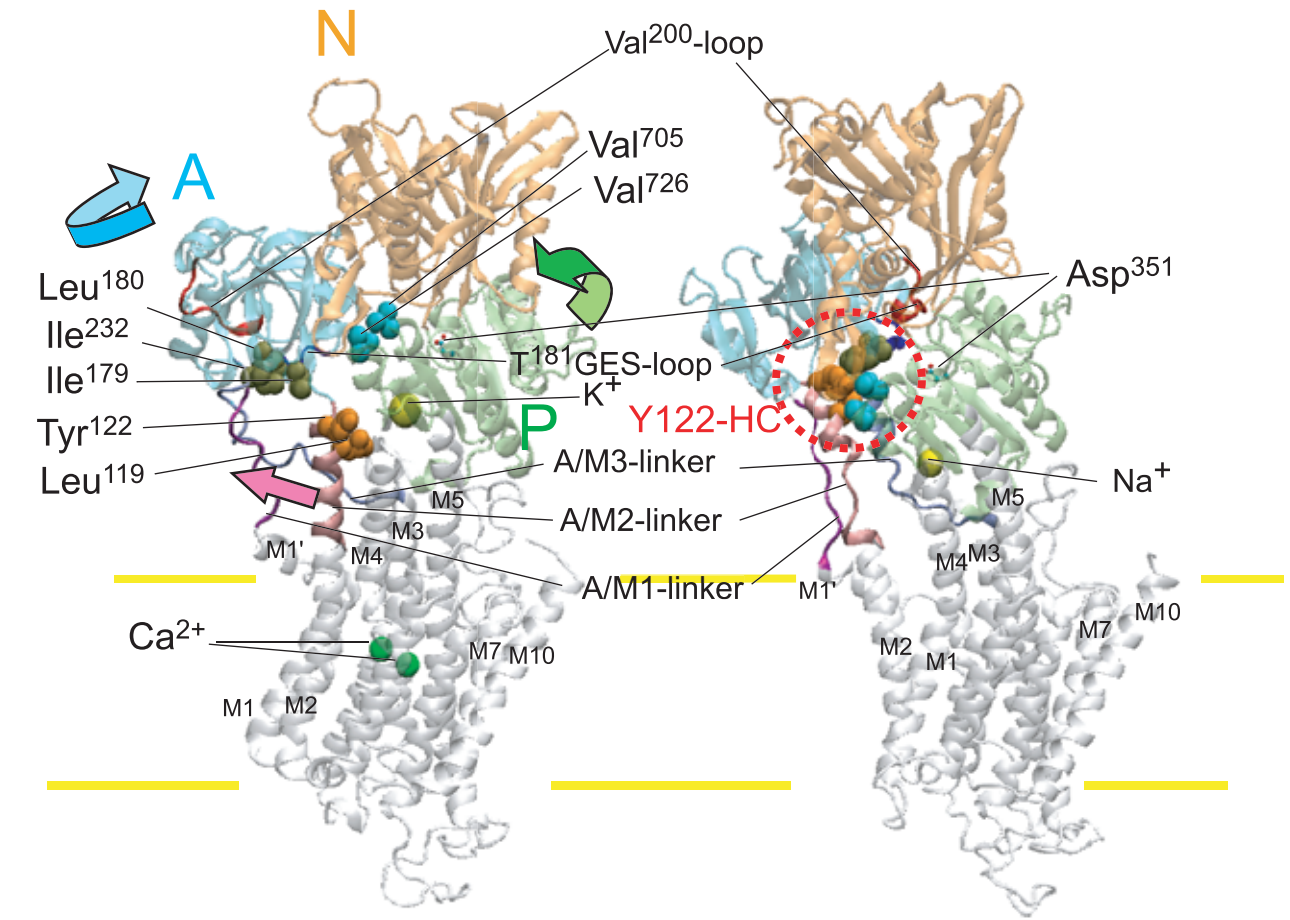
N
A
P
Val200-loop
Val705
Val726
Asp351
Leu180
Ile232
Ile179
Tyr122
Leu119
T181GES-loop
K+
Y122-HC
A/M3-linker
A/M2-linker
A/M1-linker
Na+
Ca2+
M1'
M4
M3
M5
M7
M10
M1
M2
E1~PCa2 (E1Ca2AlF4-ADP)
E2Pi (E2MgF42-)

Figure 1

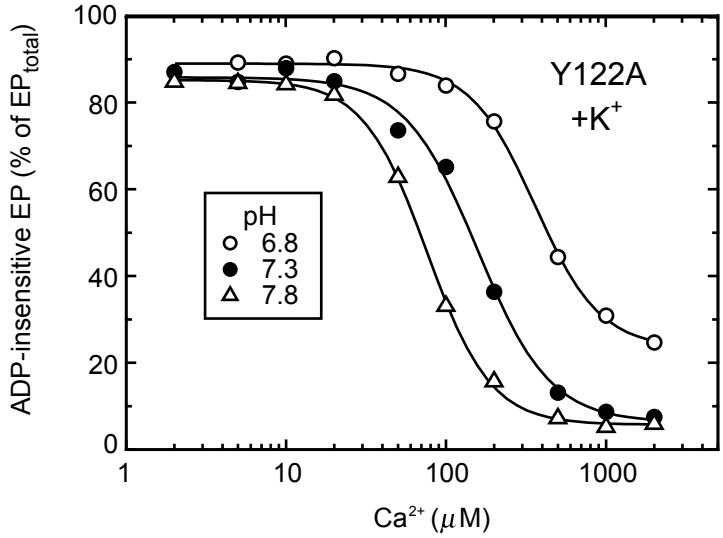
ADP-insensitive EP (% of EP$_{total}$)
100
80
60
40
20
0
1
10
100
1000
Ca^{2+} (μM)
Y122A
+K$^+$
pH
6.8
7.3
7.8

Figure 2

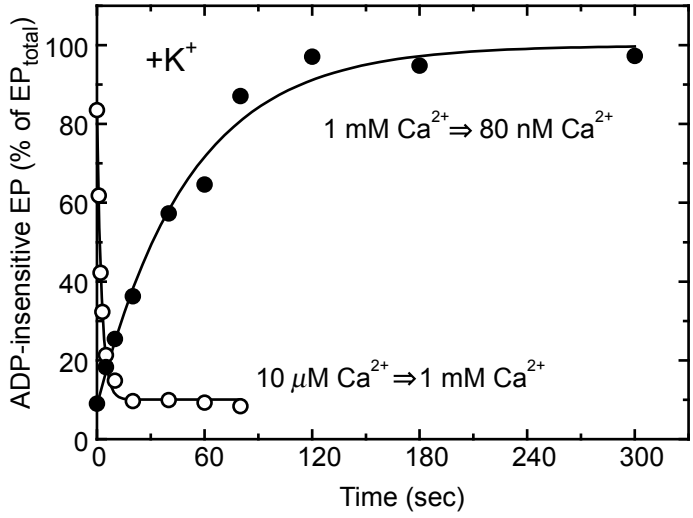
ADP-insensitive EP (% of EP$_{total}$)
100
80
60
40
20
0
+K$^+$
1 mM Ca^{2+}⇒ 80 nM Ca^{2+}
10 μM Ca^{2+}⇒1 mM Ca^{2+}
0
60
120
180
240
300
Time (sec)

Figure 3

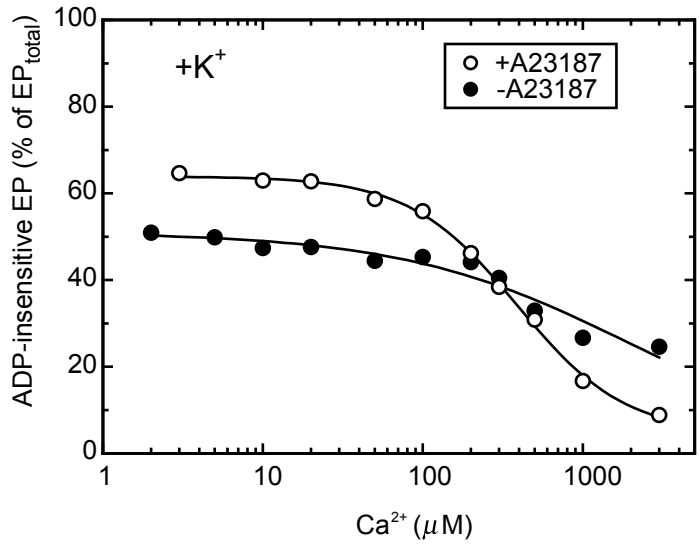
ADP-insensitive EP (% of EP$_{total}$)
100
80
60
40
20
0
1
10
100
1000
Ca^{2+} (μM)
+K$^+$
+A23187
-A23187

Figure 4

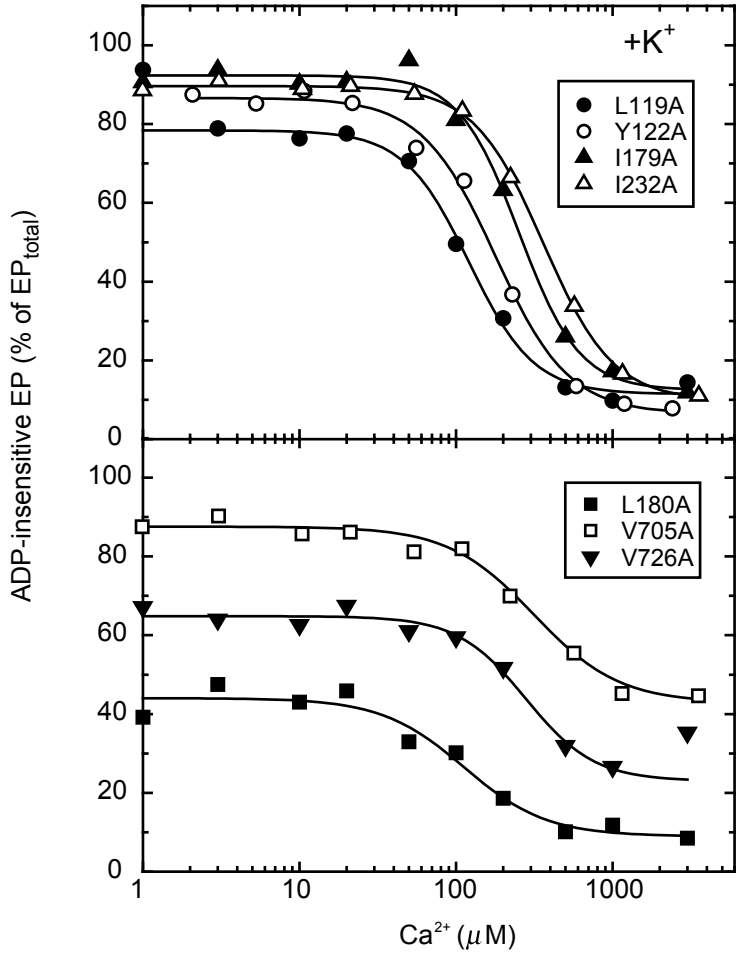
+K+
L119A
Y122A
I179A
I232A
L180A
V705A
V726A
ADP-insensitive EP (% of EPtotal)
Ca2+ (μM)
0
20
40
60
80
100
1
10
100
1000

Figure 5

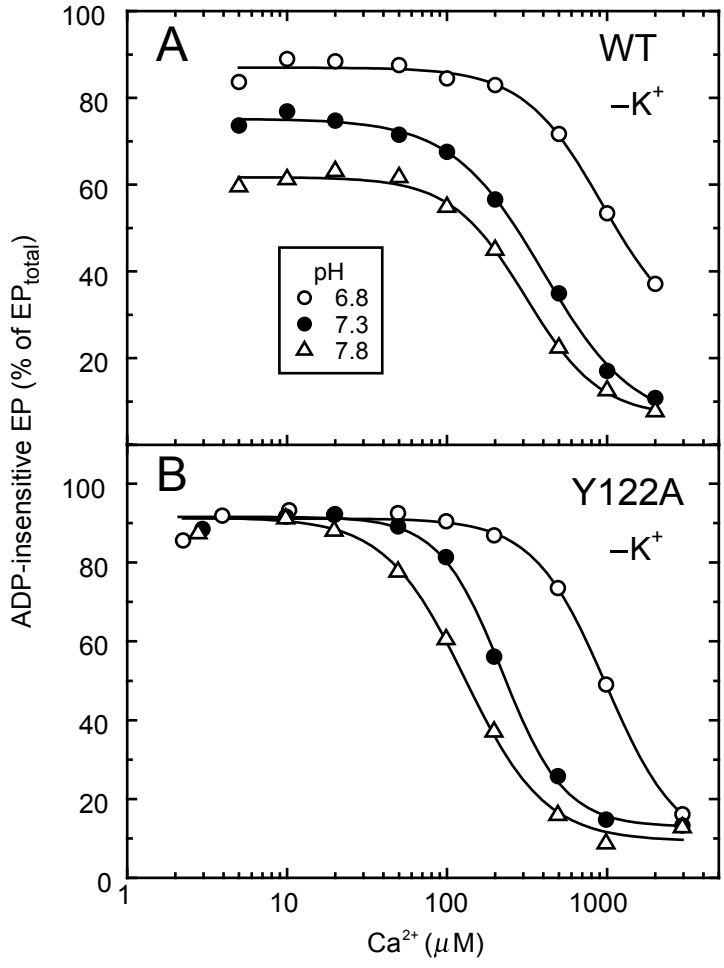
A
WT
–K+
pH
6.8
7.3
7.8
B
Y122A
–K+
ADP-insensitive EP (% of EPtotal)
Ca2+ (μM)
0
20
40
60
80
100
1
10
100
1000

Figure 6

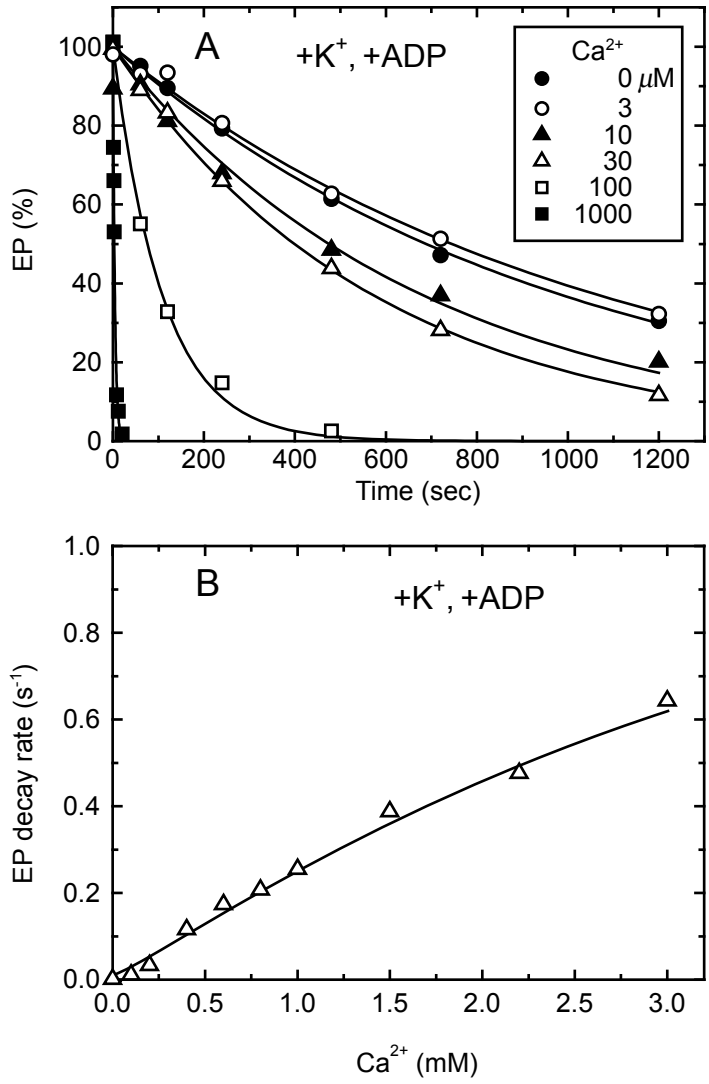
A
+K+, +ADP
Ca2+
0 μM
3
10
30
100
1000
EP (%)
Time (sec)
B
+K+, +ADP
EP decay rate (s-1)
Ca2+ (mM)

Figure 7

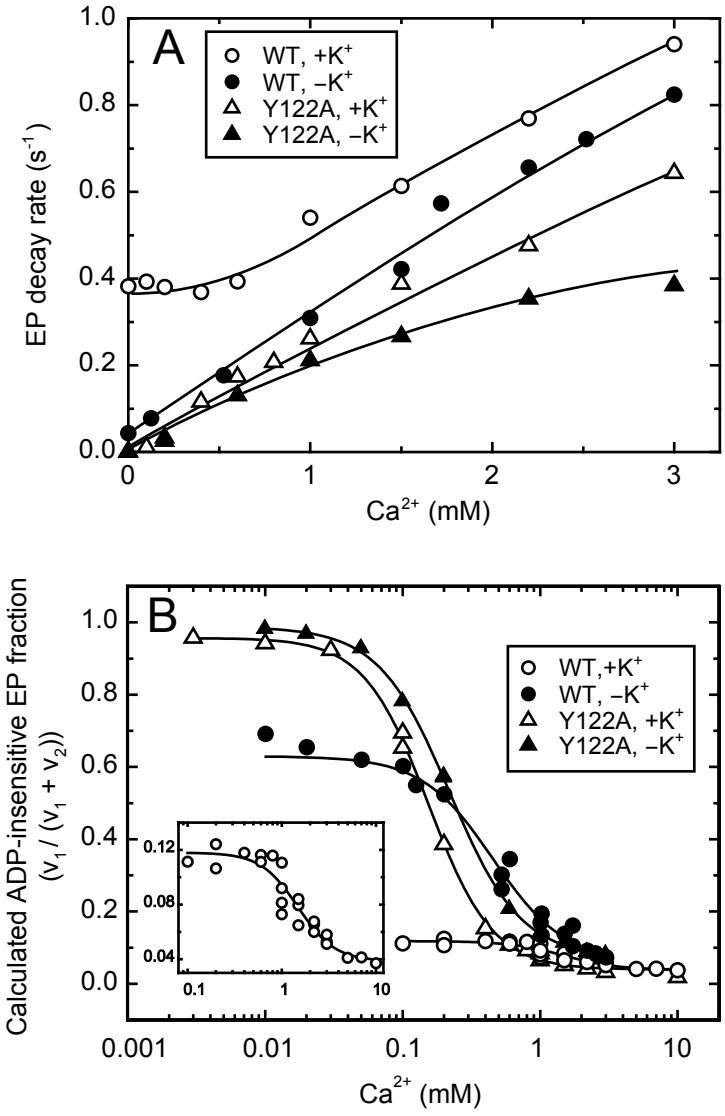
A
WT, +K+
WT, −K+
Y122A, +K+
Y122A, −K+
EP decay rate (s-1)
Ca2+ (mM)
B
WT,+K+
WT, −K+
Y122A, +K+
Y122A, −K+
Calculated ADP-insensitive EP fraction
(v1 / (v1 + v2))
Ca2+ (mM)

Figure 8

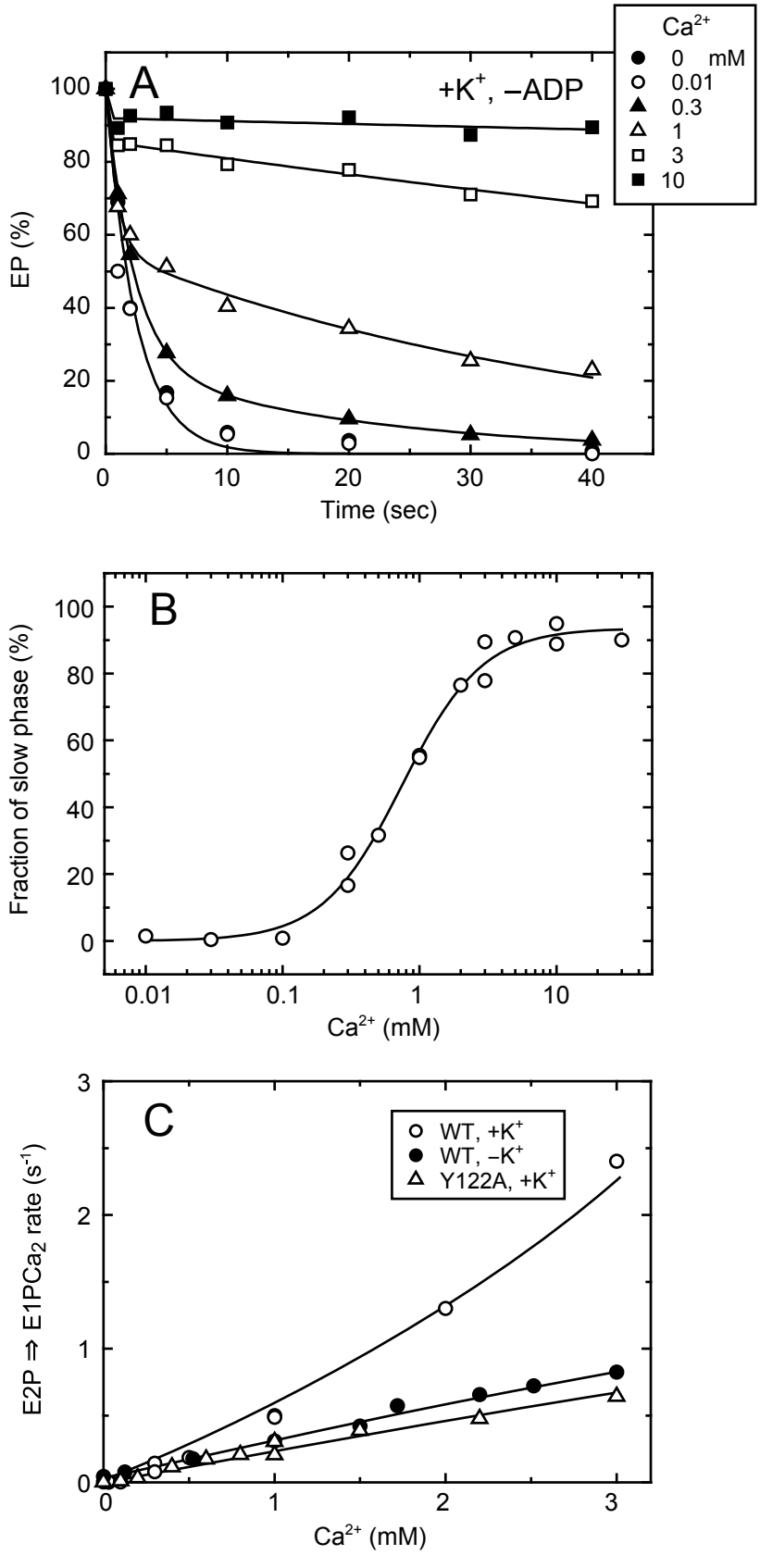
A
+K+, –ADP
Ca2+
0 mM
0.01
0.3
1
3
10
EP (%)
Time (sec)
B
Fraction of slow phase (%)
Ca2+ (mM)
C
WT, +K+
WT, –K+
Y122A, +K+
E2P ⇒ E1PCa2 rate (s-1)
Ca2+ (mM)

Figure 9

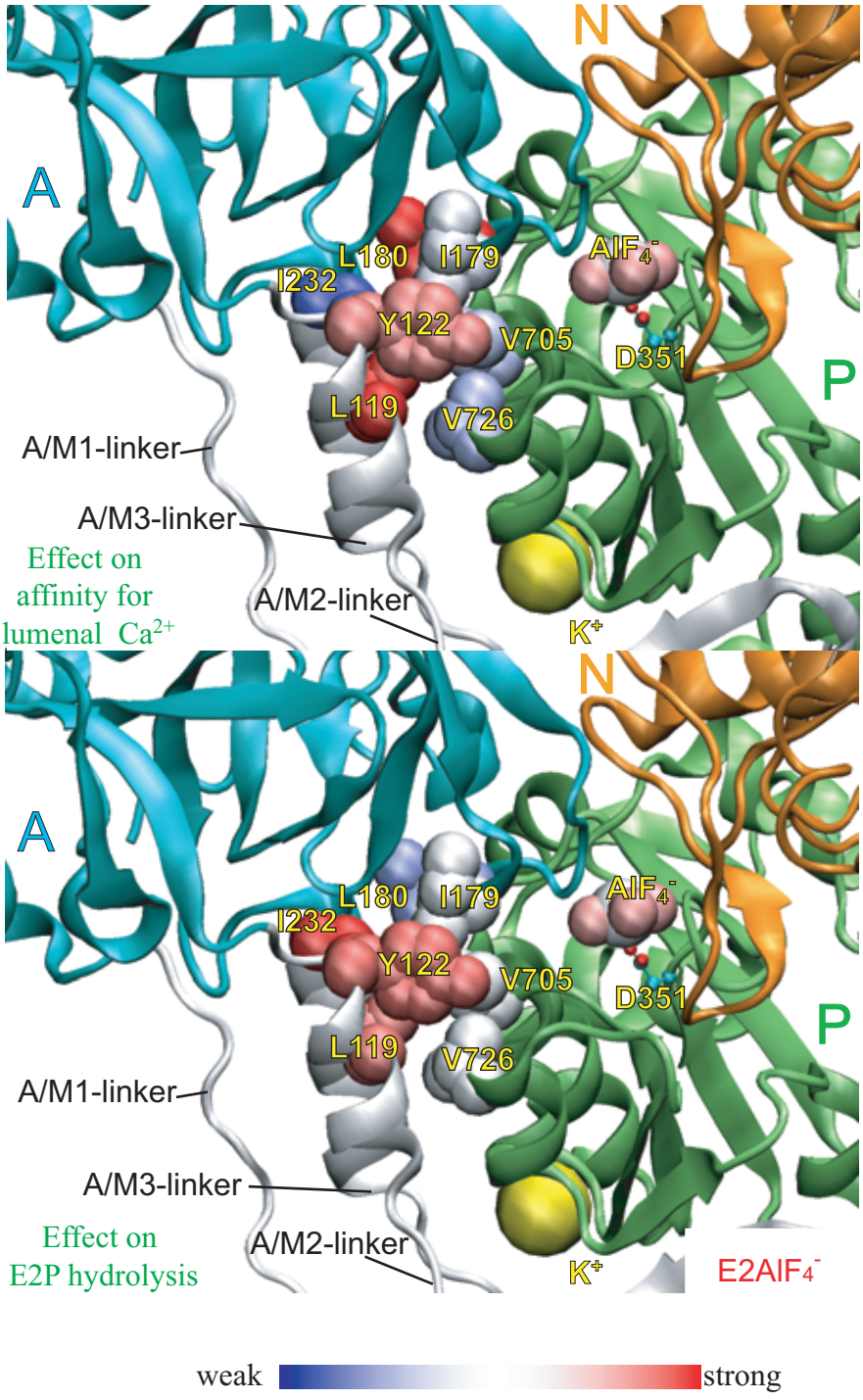
N
A
L180
I179
I232
AlF4-
Y122
V705
D351
P
L119
V726
A/M1-linker
A/M3-linker
Effect on
affinity for
lumenal Ca2+
A/M2-linker
K+
N
A
L180
I179
I232
AlF4-
Y122
V705
D351
P
L119
V726
A/M1-linker
A/M3-linker
Effect on
E2P hydrolysis
A/M2-linker
K+
E2AlF4-
weak
strong

Figure 10

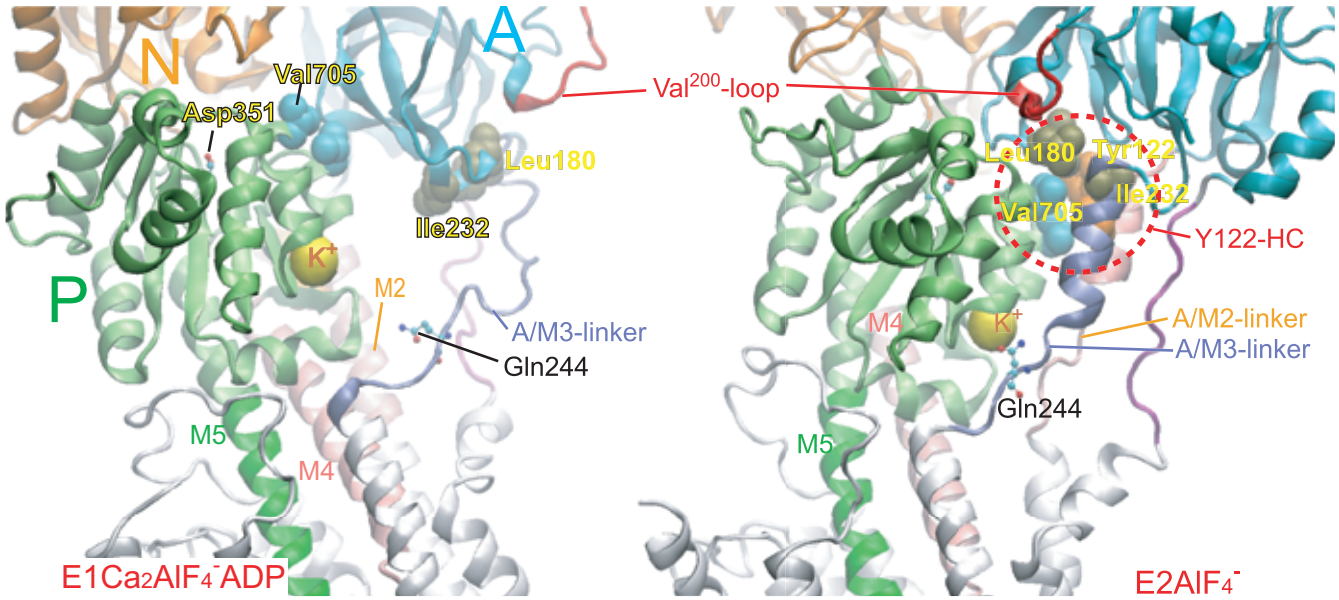
N
A
P
Val705
Asp351
Leu180
Ile232
K+
M2
A/M3-linker
Gln244
M5
M4
E1Ca2AlF4-ADP
Val200-loop
Leu180
Tyr122
Ile232
Val705
Y122-HC
M4
K+
A/M2-linker
A/M3-linker
Gln244
M5
E2AlF4-

Figure 11

SUPPLEMENTAL MATERIAL

for the manuscript by

Kazuo Yamasaki, Guoli Wang, Takashi Daiho, Stefania Danko, and Hiroshi Suzuki

Roles of Tyr^{122}-Hydrophobic Cluster and K^+ Binding in Ca^{2+}-releasing Process of ADP-insensitive Phosphoenzyme of Sarcoplasmic Reticulum Ca^{2+}-ATPase

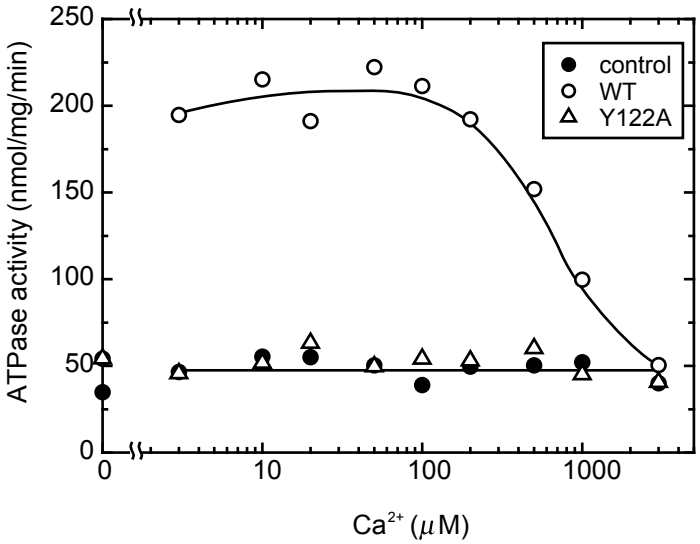

Supplemental Figure 1

Supplemental Figure 1. **ATPase activities of SERCA1a wild type and mutant Y122A at various high concentrations of Ca^{2+}.** The ATPase activities of the microsomes expressing SERCA1a wild type (WT) or mutant Y122A, and that of the control microsomes (no SERCA1a expression) were determined at various Ca^{2+} concentrations in the presence of A23187 and 7 mM $MgCl_2$ as described under "EXPERIMENTAL PROCEDURES." The points at zero Ca^{2+} indicate the activities determined without the $CaCl_2$ addition. Note that the Ca^{2+}-ATPase activity was completely inhibited in Y122A at all the Ca^{2+} concentrations. In the wild type, the reduction of the activity at the high Ca^{2+} concentrations involves not only the lumenal Ca^{2+}-induced feedback inhibition but also the marked retardation of the Ca^{2+}-ATPase cycle by the substrate CaATP produced at the high Ca^{2+} concentrations. In fact, the affinity of the enzyme for CaATP is approximately 10 times higher than that for MgATP, and the turnover rate of *E*P formed from CaATP (thus Ca^{2+} bound at the catalytic site) is far slower than that formed with MgATP (41). Therefore, even with the wild type, it is not possible to determine the lumenal Ca^{2+} affinity by this experimental design.

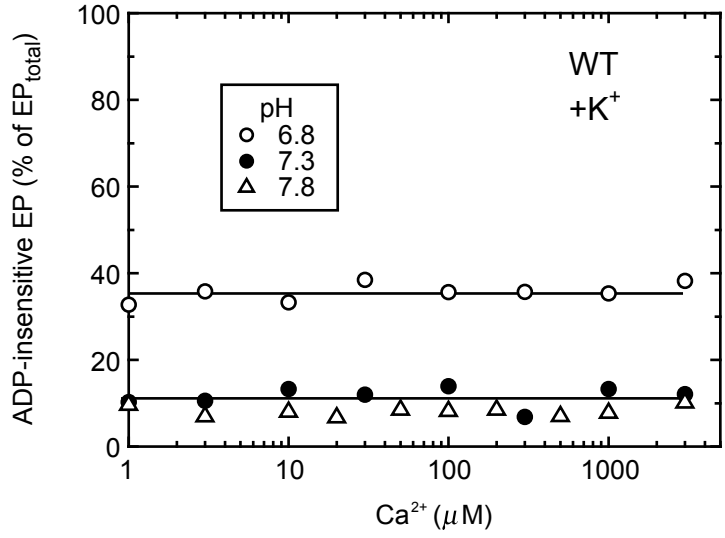

Supplemental Figure 2

Supplemental Figure 2. **Ca^{2+} dependence of accumulation of ADP-insensitive *E*P in the steady state in wild type.** The fraction of ADP-insensitive *E*P in the total amount of *E*P was determined with the wild type at various Ca^{2+} concentrations as described in Fig. 2 for the mutant Y122A.

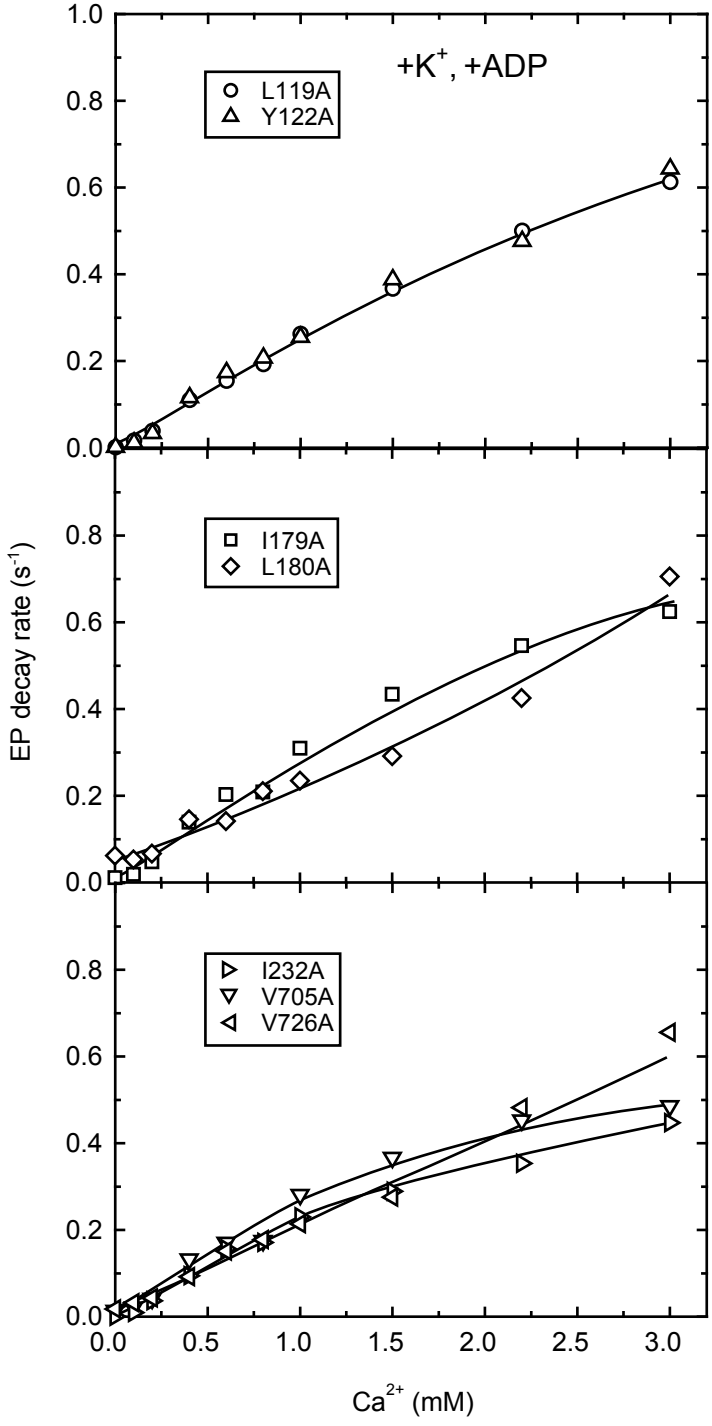

Supplemental Figure 3

Supplemental Figure 3. **Lumenal Ca^{2+}- and ADP-induced reverse *E*2P decay of Tyr^{122}-hydrophobic cluster mutants in the presence of K^+.** With all the seven Y122-HC mutants, *E*2P was first formed from $^{32}P_i$ in the absence of Ca^{2+}, and the *E*2P decay time courses upon the addition of various concentrations of Ca^{2+} and ADP were determined as described in Fig. 7*A* for the representative mutant Y122A. The single exponential decay rates thus obtained were plotted *versus* Ca^{2+} concentrations as in Fig. 7*B*.

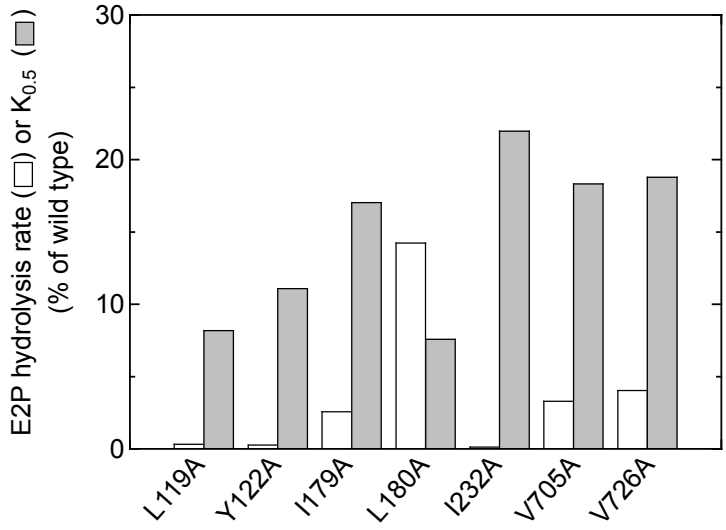

Supplemental Figure 4

Supplemental Figure 4. **Different extents of mutational effects of seven residues in Y122-HC on *E2*P hydrolysis and lumenal Ca^{2+} affinity.** The *E*2P hydrolysis rates of each of the seven mutants for Y122-HC (*open bars*) were determined in the absence of Ca^{2+} and ADP and presence of 0.1 M K^+ otherwise as in Fig. 7. The results agree with our previous study (22). The apparent affinities of *E*2P for lumenal Ca^{2+} in the presence of 0.1 M K^+ at pH 7.3 ($K_{0.5}$, *gray bars*) were determined with the seven Y122-HC mutants in Fig. 6 and estimated with the wild type in Fig. 8*B*. These values are shown as % of those of the wild type.

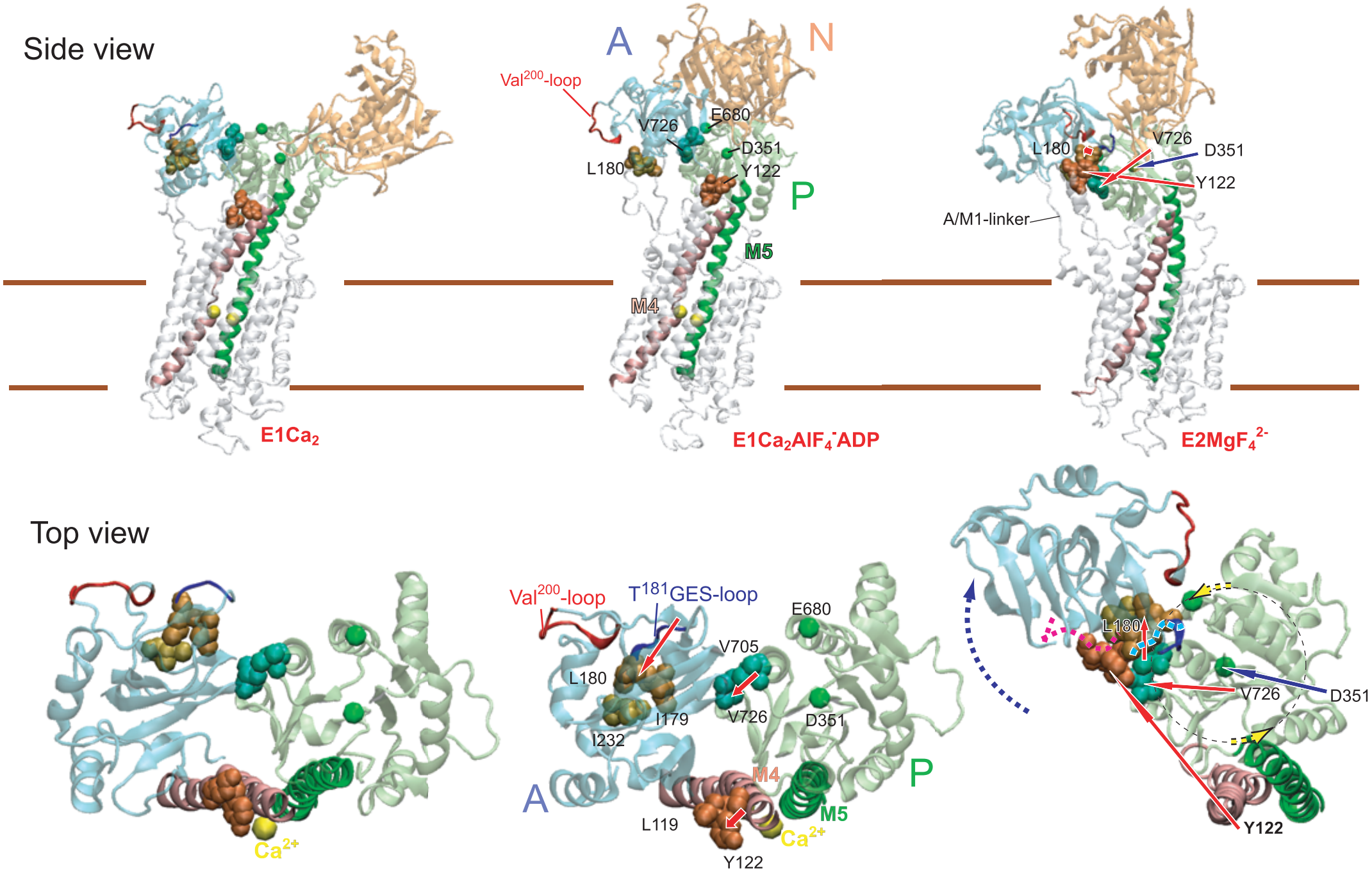

Supplemental Figure 5A

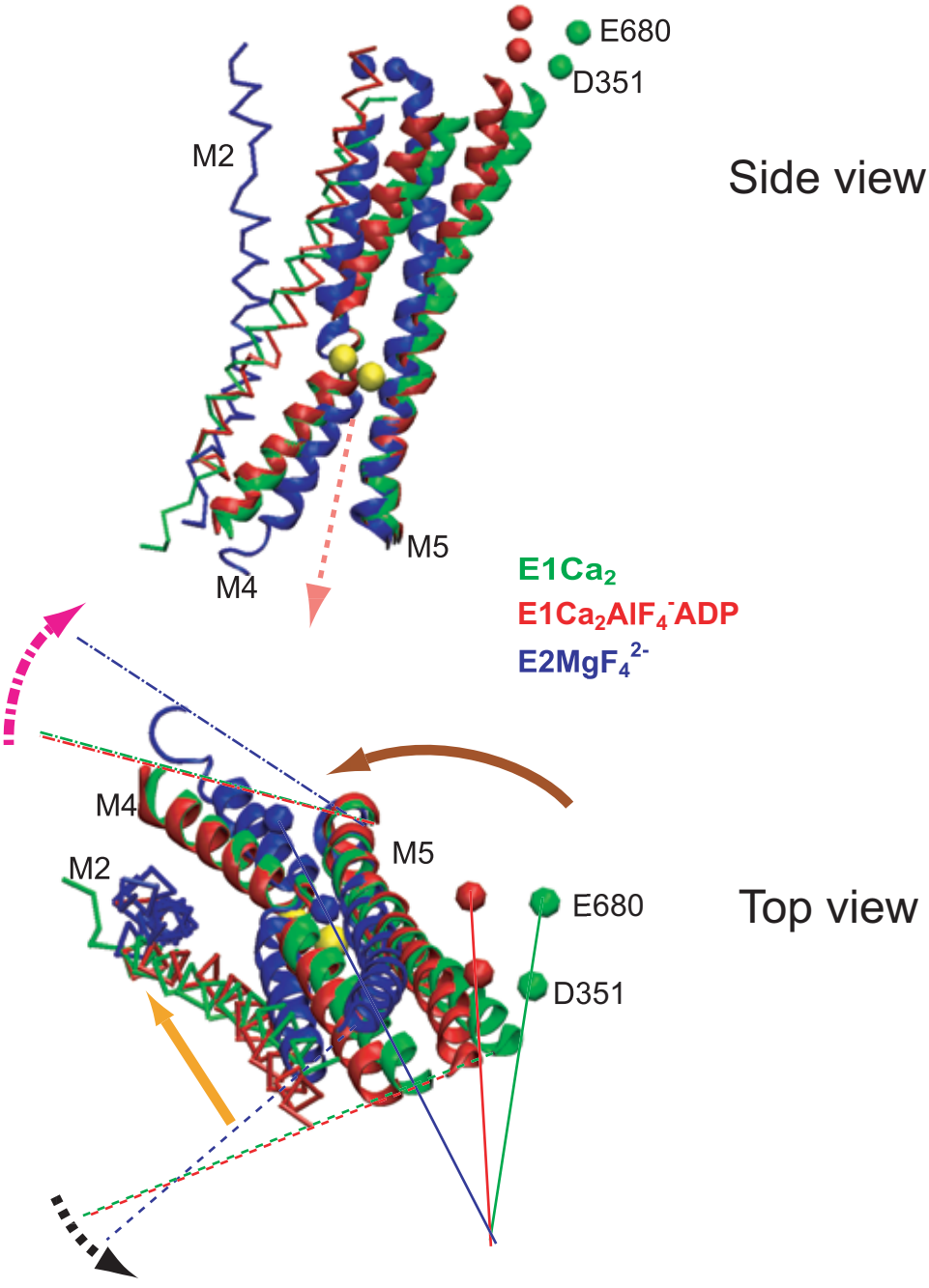

Supplemental Figure 5B

Supplemental Figure 5. **Inclination and rotational movements of P domain with twisting-like motion of M4 and M5 in *E*1PCa$_2$ → *E*2P + 2Ca^{2+}.** Three structures *E*1Ca$_2$ (PDB code; 1SU4 (10)), *E*1Ca$_2$·AlF$_4^-$·ADP (the analog for transition state *E*1~PCa$_2$·ADP (1T5T (12))), and *E*2·MgF$_4^{2-}$ (*E*2·P$_i$ analog (1WPG)) are fitted manually with M8-M10 helices.

(*A*) *Side view* of the whole molecule and *Top view* of the P and A domains, M4, and M5 from the cytoplasmic side are shown by semitransparent mode. The seven residues involved in Y122-HC (Leu^{119}/Tyr^{122}, Ile^{179}/Leu^{180}, Ile^{232}, and Val^{705}/Val^{726}) are shown by *van der Waals spheres*. The Val^{200} loop and T^{181}GES loop are depicted by *ribbon diagrams*. The alpha carbons of Asp^{351} (located approximately at the center of the P domain) and Glu^{680} (at the outermost part of this domain) were depicted by *green spheres* to show the motion of the P domain. The three *thin red arrows* on *Top view* of *E*1Ca$_2$·AlF$_4^-$·ADP show the movements of Tyr^{122}, Leu^{180}, and Val^{726}, respectively, from *E*1Ca$_2$ to *E*1Ca$_2$·AlF$_4^-$·ADP. The three *thin red arrows* on the *Side* and *Top views* of *E*2·MgF$_4^{2-}$ show the movements of these three residues from *E*1Ca$_2$·AlF$_4^-$·ADP to *E*2·MgF$_4^{2-}$ (as indicated by Y122, L180, and V726) to form Y122-HC. The *solid blue arrow* on *E*2·MgF$_4^{2-}$ shows the movement of Asp^{351} from *E*1Ca$_2$·AlF$_4^-$·ADP to *E*2·MgF$_4^{2-}$. The *dotted yellow arc arrows* on *E*2·MgF$_4^{2-}$ show the rotational motion of the P domain around Asp^{351} in the change from *E*1Ca$_2$·AlF$_4^-$·ADP to *E*2·MgF$_4^{2-}$; note that the *dotted yellow arc arrow* placed on Glu^{680} (*green sphere*) actually indicates the approximate movement of this residue in the change. In *E*2·MgF$_4^{2-}$, Glu^{680} is located in the immediate vicinity of the Val^{200} loop and actually involved in the ionic interactions with this loop. The *dotted blue arc arrow* on *E*2·MgF$_4^{2-}$ shows the rotational movement of A domain from *E*1Ca$_2$·AlF$_4^-$·ADP to *E*2·MgF$_4^{2-}$ around the T^{181}GES-loop region. The *dotted pink* and *light blue ribbons* superimposed on *E*2·MgF$_4^{2-}$ indicate the locations of the Val^{200}- and T^{181}GES-loops in *E*1Ca$_2$·AlF$_4^-$·ADP, respectively; the Val^{200} loop, the outermost loop of the A domain, largely moves and comes to the interface with the P domain at Glu^{680} as the A domain largely rotates around the T^{181}GES-loop region.

(*B*) M4 and M5 (*solid ribbons*), M2 (*trace of its alpha carbons*), and the alpha carbons of Asp^{351} and Glu^{680} (*van der Waals spheres*) are exhibited in the three structures; *E*1Ca$_2$ (*green*), *E*1Ca$_2$·AlF$_4^-$·ADP (*red*), and *E*2·MgF$_4^{2-}$ (*blue*). The three structures are fitted manually with M8-M10. The *Side view* and *Top view* from the cytoplasmic side are shown. The two Ca^{2+} ions bound in *E*1Ca$_2$·AlF$_4^-$·ADP are shown by *yellow van der Waals spheres*, and its release into lumen is roughly shown by *dotted salmonpink arrow* on *Side view*. On *Top view*, the three *thin solid lines* are drawn from Glu^{680} (the outermost part of the P domain) through Asp^{351} (the approximate center of the P domain) to show their alignment in each of the three structures and thus to depict the rotational motion of the P domain (*brown solid arc arrow*) in the change from *E*1Ca$_2$ to *E*1Ca$_2$·AlF$_4^-$·ADP and further to *E*2·MgF$_4^{2-}$. The three *broken thin lines* are drawn from the cytoplasmic top part of M5 (Phe^{740}) through that of M4 (Lys^{329}), and three *dash-dotted thin lines* are from the lumenal end of M5 (Leu^{781}) through that of M4 (Ile^{289}). These two sets of the three lines are to depict the motions of M4 and M5 at the cytoplasmic part (*black broken arc arrow*) and at the lumenal end (*magenta dash-dotted arc arrow*) in the change

from $E1Ca_2$/$E1Ca_2$·AlF_4^-·ADP to $E2{\cdot}MgF_4^{2-}$. The *orange solid arrow* shows the movement of Tyr^{122} on the cytoplasmic top part of M2 in the change from $E1Ca_2$/$E1Ca_2$·AlF_4^-·ADP to $E2{\cdot}MgF_4^{2-}$.

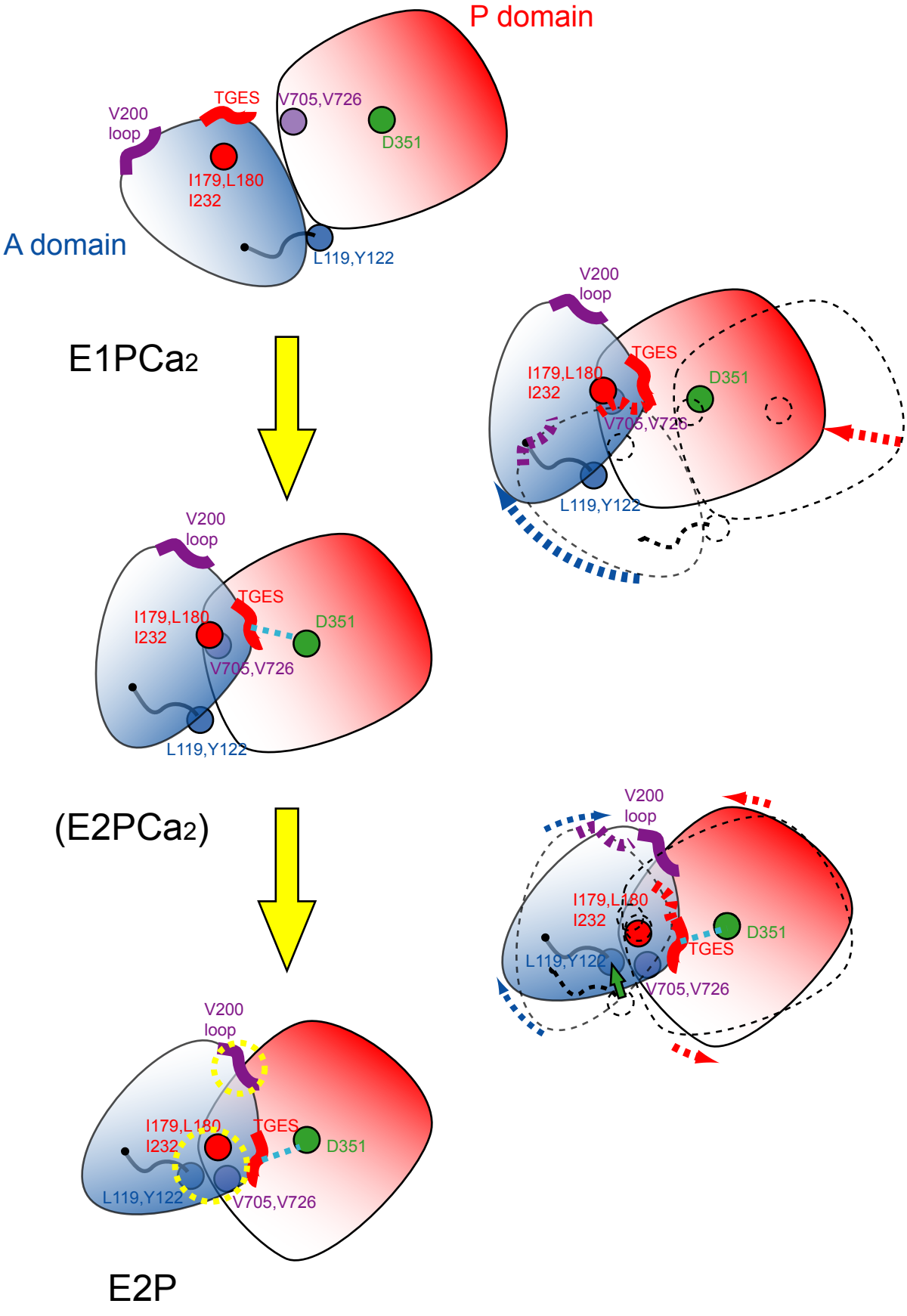

Supplemental Figure 6

Supplemental Figure 6. **Schematic model for rearrangement of P and A domains for *E*P isomerization and Ca^{2+} release**. Depicted is our schematic model for the motions of the A and P domains in the successive two steps (*large yellow arrows*); *E*1PCa_2 → *E*2PCa_2 (loss of the ADP-sensitivity) and *E*2PCa_2 → *E*2P + $2Ca^{2+}$ (Ca^{2+} release). The model is made on the basis of the observed mutational effects of Y122-HC and Val^{200} loop (22-24). The top view from the cytoplasmic side is shown (as in *Top view* of Supplemental Figure 3A). The P and A domains, Val^{200} loop, T^{181}GES loop, and Asp^{351} in *E*1PCa_2 and *E*2P are positioned according to the structures of *E*1Ca_2·AlF_4^-·ADP (1T5T) and *E*2·MgF_4^{2-} (1WPG), respectively. *E*2PCa_2 is the postulated intermediate state. The positions of the seven residues involved in Y122-HC in the three regions are shown by the representative ones (Y122, L180, and V705). In the pictures placed for the two *large yellow arrows*, the structure (*broken lines*) before its change was superimposed on that after the change, and the motions of the A and P domains are indicated by *dotted blue arrow* and *dotted red arrow*, respectively.

*E*1PCa_2 → *E*2PCa_2; the loss of ADP-sensitivity:

The A domain rotates largely (probably due to the strain of the A/M3-linker) around the T^{181}GES loop and the P domain inclines to some extent toward the A domain, thereby the T^{181}GES loop docks onto the Asp^{351}-region producing hydrogen-bonding interactions (*dotted blue line*), hence causing the loss of the ADP-sensitivity (the T^{181}GES loop blocks the access of ADP *β*-phosphate to Asp^{351}-acylphosphate). In this state, the two interaction networks at Y122-HC and at the Val^{200} loop are not yet fully produced. Our previous mutation study on the interaction network between Arg^{334}/Arg^{324} of the P domain and top part of M2 (Glu^{123}/Tyr^{122}/Glu^{121}/Glu^{117}/Asn^{114}/Glu^{113}/Asn^{111}/Glu^{109}/Gln^{108}) indicated (22) that the inclination of the P domain occur at least to some extent along this interaction network for the loss of the ADP-sensitivity, *E*1PCa_2 → *E*2PCa_2.

*E*2PCa_2 → *E*2P + $2Ca^{2+}$; Ca^{2+} release after the loss of ADP-sensitivity:

The P and A domains further rotate slightly in the opposite directions and the top part of M2 (Tyr^{122}/Leu^{119}) likely moves more (*green solid arrow*), thereby they produce the interactions fully at Y122-HC and at Val^{200} loop (*dotted yellow circles*) so as to realize and stabilize the Ca^{2+}-released structure of *E*2P. The native and appropriately short length of the A/M1-linker (its strain) critically contributes to the structural changes for Ca^{2+}-deocclusion/release and formation of Y122-HC in *E*2PCa_2 → *E*2P + $2Ca^{2+}$; in this case, especially for the vertical motions of the P and A domains and M4/M5, and the inclination of M2. These vertical factors are not depicted in this top view.

Upon these changes, the catalytic site is rearranged to produce its appropriate configuration for the subsequent Asp^{351}-acylphosphate hydrolysis, *e.g.* the T^{181}GES loop comes to the position where the Glu^{183}-coordinated water molecule can attack Asp^{351}-acylphosphate. Hence in this structural mechanism, the possible hydrolysis without releasing Ca^{2+} is avoided, and the Ca^{2+} release and the subsequent *E*2P hydrolysis are accomplished as the ordered sequence.

In the wild type, all these successive structural events in *E*1PCa_2 → *E*2PCa_2 → *E*2P + $2Ca^{2+}$ occur in coordinated manner and thus rapidly; therefore *E*2PCa_2 does not accumulate stably in the wild type.